1

Self-Assembly from Surfactants to Nanoparticles – Head vs. Tail

Ramanathan Nagarajan

Natick Soldier Research, Development & Engineering Center,
15 General Greene Avenue, Natick MA 01760, USA

1.1 Introduction

Surfactant molecules are amphiphilic, composed of a polar headgroup that likes water and a nonpolar tail that dislikes water, thus contributing to an intrinsic duality in their molecular characteristics. Despite their mutual antipathy, the headgroup and tail of the surfactant cannot leave one another because they are covalently connected. The dilemma of mutual antipathy and forced coexistence faced by these molecules is resolved in nature by the intriguing phenomenon of molecular self-assembly, wherein the surfactant molecules self-assemble into three-dimensional structures with distinct and separate regions composed of the nonpolar parts and the polar parts, having minimal contact with one another. Block copolymers are an important class of high molecular weight polymer molecules that share great molecular similarity with the surfactants. A diblock copolymer is made up of repeating units A and B, with the repeating units occurring as blocks, covalently connected to one another. If one block (B) is hydrophilic or solvophilic (head) while the other block (A) is hydrophobic or solvophobic (tail), the block copolymer becomes a high molecular weight analog of the low molecular weight surfactant. Surfactants and block copolymers display characteristic molecular self-assembly behavior in solutions, at interfaces as well as in bulk, generating nanoscale structures of different shapes. These nanoscale features determine many macroscopic properties of these amphiphile systems, relevant for their practical applications.

The ability to generate desired nanoscale morphologies by synthesizing novel amphiphiles so that the amphiphilic systems can be tailored for specific applications as well as the ability to manipulate the morphologies using chemical and physical stimuli remain active goals of research in this field. Critical to

Self-Assembly: From Surfactants to Nanoparticles, First Edition. Edited by Ramanathan Nagarajan.

achieving these goals is an understanding of the link between the molecular structure of the amphiphiles and their self-assembly behavior. Studies on surfactants have a long history, starting with the pioneering recognition of the existence of aggregates of soap molecules by McBain [1], over 100 years ago. He coined the term micelles to describe these aggregates and visualized a lamellar morphology for these aggregates. The proposal of a spherical micelle structure was made by Hartley [2] who suggested that the "aggregates are essentially liquid and since they will tend to present the minimum surface to the water, they will presumably be roughly spherical and of the largest radius consistent with none of the heads being submerged in the paraffin interior." Theoretical developments relating to surfactants have a rich history of 70 years starting with a pioneering model proposed by Debye [3]. The historical developments in the evolution of theories applied to surfactants leading up to current state of the art have recently been summarized [4].

The first synthesis of block copolymers was reported by Dunn and Melville [5] who synthesized and characterized a diblock copolymer of poly(methyl methacrylate)-b-poly(styrene). The observation that solvents can cause segregation of polymer blocks was first made by Merrett [6] based on studies of graft copolymers with rubber as backbone and grafted blocks of poly(methyl methacrylate) interacting with solvent mixtures involving benzene and methanol, benzene being a good solvent for rubber and methanol a good solvent for poly(methyl methacrylate). Merrett also used the term micelle to describe the graft copolymer aggregates. The first report of block copolymer aggregates in solution was from Climie and White [7] who studied poly(methyl methacrylate)-b-poly (acrylonitrile) in a mixed solvent of dimethyl formamide, which is a good solvent for both blocks and benzene, which is a nonsolvent for the poly(acrylonitrile) block. The clear demonstration of block copolymer micelles formed in dilute solutions was reported by Krause [8]. In this study using poly(styrene)-b-poly(methyl methacrylate) block copolymer, micelles were obtained in acetone, a non-solvent for poly(styrene), and in triethylbenzene, a nonsolvent for poly(methyl methacrylate). Block copolymer aggregates thus have a rich history of nearly 60 years and these early developments along with a comprehensive discussion of the synthesis and solution properties of block copolymers have been reviewed some years ago by Riess [9].

In this chapter, we focus mainly on the theoretical ideas based on which quantitative models to describe the self-assembly of surfactants and block copolymers have been developed. Tanford [10] and Israelachvili et al. [11] pioneered two of the most important models that currently dominate our understanding of surfactant self-assembly. Tanford proposed the concept of opposing forces to formulate a quantitative expression for the standard free energy change when a singly dispersed surfactant molecule in solution becomes part of a multimolecular surfactant aggregate, also in the solution. In his model, the formation of the equilibrium aggregate resulted from balancing the interfacial free energy

at the micelle-water interface against the repulsions between the surfactant headgroups also located at the interface. Using this free energy expression, with the controlling role played by the headgroup, he was able to explain why surfactant aggregates form in aqueous solutions, why they grow, and why they do not keep growing but remain finite in size. Israelachvili, Mitchell, and Ninham proposed the concept of a molecular packing parameter P defined as $P = v_o/a_e\ell_o$, where v_o and ℓ_o are the volume and length of the surfactant tail and a_e is the equilibrium area per molecule of the surfactant aggregate at the hydrophobic core-water interface. They demonstrated how the size and the shape of the aggregate at equilibrium can be predicted from the magnitude of P in accordance with simple geometry driven molecular packing considerations. In the context of the Tanford model, P is mainly dependent on the headgroup interactions and therefore the aggregate size and shape predicted by the packing parameter are clearly dominated by only the headgroup interactions. Remarkably, in this model, the surfactant tail has no explicit role in influencing the aggregate shapes.

Theoretical studies of self-assembly of block copolymers evolved without any obvious contact with the surfactant self-assembly literature. Theoretical understanding of how pure block copolymers organize into microdomains was advanced through the work of Meier [12, 13] and Helfand [14, 15]. Theoretical treatments of block copolymer micelles in selective solvents or in homopolymers have been pioneered by de Gennes [16], Leibler et al. [17], Noolandi and Hong [18], and Whitmore and Noolandi [19]. de Gennes [16] analyzed the formation of a diblock copolymer micelle in selective solvents by minimizing the free energy per molecule of an isolated micelle with respect to the aggregation number or core radius. The micelle core was assumed fully segregated and devoid of any solvent. In this model framework, the free energy of formation of the core-corona interface and the elastic free energy of stretching of the core blocks compete to control the micellization behavior. Leibler et al. [17] treated the problem of micelle formation of a symmetric diblock copolymer in a homopolymer solvent. In their study, as in de Gennes' work, the interface was taken to be sharp. Noolandi and Hong [18] and Whitmore and Noolandi [19] formulated mean field models taking into account the possibility of a diffuse interface between the core and corona regions. In all treatments of block copolymer self-assembly, the elastic deformation of the core forming block (the tail) played the central role. Notably, in these models, the solvophilic block (the analog of surfactant headgroup) had no explicit role. In Section 1.2 we outline the models for surfactants and block copolymers and then show how the mutually exclusive emphasis on headgroup or tail has now given place to consideration of both head and tail, thereby improving their quantitative predictive abilities. In Section 1.3 we show that the headgroup vs. tail-based free energy concepts can rationalize self-assembly behavior

observed in many non-classical amphiphile systems involving dendrimers, DNA, peptides, proteins, and nanoparticles as head or tail components.

1.2 Classical Surfactants and Block Copolymers

1.2.1 Tanford Model for Surfactant Micelles

Surfactant molecules self-assemble into spherical, globular or cylindrical micelles, or spherical bilayers, also known as vesicles (Figure 1.1). In these aggregates, the hydrophobic domain is made up of the surfactant tails and the hydrophilic headgroups are crowded at the aggregate core-water interface.

If the density in the hydrophobic domain is considered equal to that in similar liquid hydrocarbons, the surfactant tails must entirely fill the space in these domains. As a result, irrespective of the shape of the aggregate, no point within the aggregate can be farther than ℓ_o from the aggregate-water interface, where ℓ_o is the extended length of the surfactant tail. Therefore, at least one dimension of the surfactant aggregates should be smaller than or at most equal to $2\ell_o$. This is purely a geometrical or packing constraint that the surfactant aggregate will have to satisfy [10, 11]. The geometrical relations governing these different aggregate shapes are summarized in Table 1.1.

The size and shape of the aggregates are dependent on the surfactant molecular structure as well as the solution conditions. The Gibbs equilibrium condition

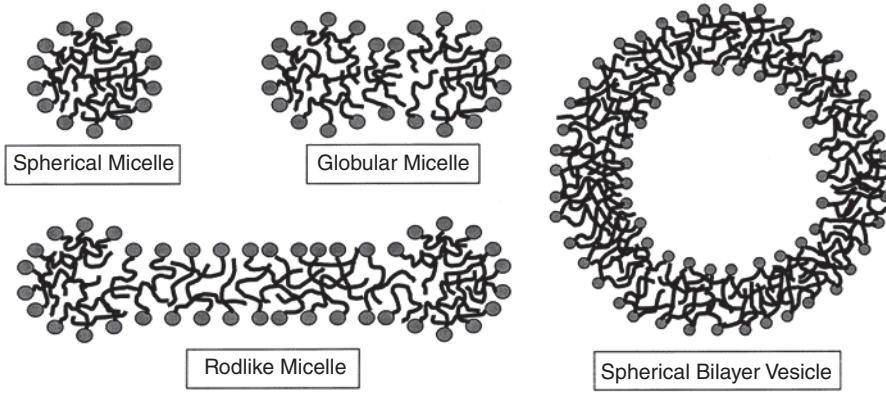

Figure 1.1 Schematic representation of surfactant aggregates in dilute aqueous solutions. The structures include spherical micelles, globular micelles not much larger than the spherical micelles, large cylindrical micelles with globular endcaps, and spherical bilayer vesicles. The length of the surfactant tail constrains one characteristic dimension in each of these aggregates (radius for the micelles and half-bilayer thickness for the vesicles). More complex aggregates involving branching of cylindrical micelles and network formation among them are discussed in detail by Victorov in Chapter 2 of this book.

Table 1.1 Geometrical relations for spherical and cylindrical micelles and bilayers.[a)]

Variable	Sphere	Cylinder	Planar bilayer
Volume of core $V = g\, v_o$	$4\pi\, R^3/3$	$\pi\, R^2$	$2R$
Surface area of core $A = g\, a$	$4\pi\, R^2$	$2\pi\, R$	2
Area per molecule a	$3v_o/R$	$2v_o/R$	v_o/R
Aggregation number g	$36\pi v_o^2/a^3$	$4\pi v_o/a^2$	$2/a$

a) R is the core radius in case of spherical, globular or cylindrical micelles and in the case of bilayer, it represents the half-bilayer thickness. g denotes the number of surfactant molecules in the aggregate. v_o is the volume and ℓ_o is the extended length of the surfactant tail. The variables V, A, and g refer to the entire aggregate in the case of a sphere, unit length in the case of a cylinder or unit area in the case of a bilayer.

stipulates the equality of chemical potential of a surfactant molecule present in the singly dispersed state and that incorporated within a multimolecular aggregate of any given size and shape [10]. This chemical potential equality allows one to relate the concentration X_g of surfactant aggregates of size g and any shape to the concentration X_1 of the singly dispersed surfactant through the equation

$$X_g = X_1^g \exp(-\mathrm{g}\, \Delta\mu_g^o/kT), \quad \Delta\mu_g^o = \frac{\mu_g^o}{g} - \mu_1^o \tag{1.1}$$

where, μ_g^o is the standard state chemical potential of an isolated micelle of aggregation number g while μ_1^o is the standard state chemical potential of a singly dispersed surfactant, both in bulk solvent. k is the Boltzmann constant and T is the temperature. Based on Eq. (1.1), the fundamental quantity of interest that will allow one to determine all aggregation properties is the standard state chemical potential difference $\Delta\mu_g^o$, also referred to as the standard free energy change on aggregation. Tanford [10, 20] formulated a quantitative expression for $\Delta\mu_g^o$ on phenomenological grounds, invoking the concept of opposing forces. The standard free energy change is composed of three contributions:

$$\left(\frac{\Delta\mu_g^o}{kT}\right) = \left(\frac{\Delta\mu_g^o}{kT}\right)_{Tail} + \left(\frac{\Delta\mu_g^o}{kT}\right)_{Int} + \left(\frac{\Delta\mu_g^o}{kT}\right)_{Head} \tag{1.2}$$

The first term $(\Delta\mu_g^o/kT)_{Tail}$ is a negative free energy contribution arising from the transfer of the surfactant tail from its unfavorable contact with water to the favorable hydrocarbon-like environment of the aggregate core. This transfer free energy contribution depends on the surfactant tail but not on the aggregate shape or size. The second term $(\Delta\mu_g^o/kT)_{Int}$ is a positive free energy contribution that accounts for the residual contact between the surfactant tails and water at the aggregate core-water interface. This is represented as the product of a contact free energy per unit area σ (or an interfacial free energy per unit area,

or interfacial tension) and the surface area per molecule of the aggregate core, a. The third term $(\Delta\mu_g^o/kT)_{Head}$ is another positive free energy contribution that accounts for the repulsive interactions between the headgroups because they crowd at the aggregate surface. The repulsions may be due to steric interactions (for any type of headgroup) and also electrostatic interactions (dipole–dipole interactions for zwitterionic headgroups and ion–ion repulsions for ionic headgroups). Since the repulsions would increase if the headgroups come close to one another, Tanford proposed an expression for this free energy contribution with an inverse dependence on a. Thus, the standard free energy change per molecule on aggregation proposed by Tanford has the form:

$$\left(\frac{\Delta\mu_g^o}{kT}\right) = \left(\frac{\Delta\mu_g^o}{kT}\right)_{Tail} + \left(\frac{\sigma}{kT}\right)a + \left(\frac{\alpha}{kT}\right)\frac{1}{a} \tag{1.3}$$

where α represents the headgroup repulsion parameter. One may note that this phenomenological parameter α has to be connected to the surfactant headgroup features and solution conditions if one wants to carry out any predictive computations of aggregation.

From the free energy model of Tanford, the equilibrium aggregation behavior can be examined either by treating the surfactant solution as consisting of aggregates with a distribution of sizes (as represented by Eq. (1.1)) or by treating the aggregate as constituting a pseudophase. If the aggregate is viewed as a pseudophase, in the sense of small systems thermodynamics, the equilibrium condition corresponds to a minimum in the standard free energy change per molecule, $\Delta\mu_g^o/kT$. The minimization can be done with respect to either the aggregation number g or the core surface area per molecule a, since they are dependent on one another through the geometrical relations given in Table 1.1. One obtains, in this manner, the equilibrium core surface area a_e per molecule characterizing the aggregate:

$$\frac{\partial}{\partial a}\left(\frac{\Delta\mu_g^o}{kT}\right) = \left(\frac{\sigma}{kT}\right) - \left(\frac{\alpha}{kT}\right)\frac{1}{a^2} = 0, at\ a = a_e \quad \Rightarrow \quad a_e = \left(\frac{\alpha}{\sigma}\right)^{1/2} \tag{1.4}$$

The critical micelle concentration (cmc, denoted as X_C in mole fraction units), in the pseudophase approximation, is obtained from the relation,

$$ln\, X_C = \left(\frac{\Delta\mu_g^o}{kT}\right)_{Tail} + \left(\frac{\sigma}{kT}\right)a_e + \left(\frac{\alpha}{kT}\right)\frac{1}{a_e} = \left(\frac{\Delta\mu_g^o}{kT}\right)_{Tail} + \left(\frac{2\sigma^{1/2}\alpha^{1/2}}{kT}\right) \tag{1.5}$$

The principal outcomes from the free energy model are the equilibrium area per molecule and the cmc. From the equilibrium area per molecule, one can

determine the shape of the aggregate based on purely geometrical considerations. For example, if we consider a spherical micelle of core radius R, made up of g molecules, the volume of the core $V = g\, v_o = 4\pi\, R^3/3$, the surface area of the core $A = g\, a = 4\pi\, R^2$, and hence $R = 3\, v_o/a$. Introducing the constraint that the core radius R cannot exceed the extended length ℓ_o of the tail, one obtains the limit, $0 \leq v_o/a\ell_o \leq 1/3$, for spherical micelles. This dimensionless group $v_o/a\ell_o$ is well known as the molecular packing parameter P, first explicitly introduced by Israelachvili et al. [11]. The application of this idea to other aggregate shapes using the geometrical relations given in Table 1.1, leads to the well-known [11] connection between the molecular packing parameter and the aggregate shape: $0 \leq v_o/a\ell_o \leq 1/3$ for sphere, $1/3 \leq v_o/a\ell_o \leq 1/2$ for cylinder, and $1/2 \leq v_o/a\ell_o \leq 1$ for bilayer. The ratio v_o/ℓ_o is a property of the surfactant tail and since both the volume and length are proportional to the number of carbon atoms in an aliphatic tail, the ratio v_o/ℓ_o is a constant, practically independent of the tail length, equal to $0.21\,\text{nm}^2$ for single-chain surfactants and $0.42\,\text{nm}^2$ for double-chain surfactants. Therefore, once the equilibrium area is determined from the Tanford free energy model, one can identify the size and shape of the aggregate and the magnitude of the cmc.

In the Tanford free energy expression (Eq. (1.3)), only the first contribution, the tail transfer free energy, is negative, and this allows the free energy change on aggregation to be negative. Hence, this contribution is solely responsible for the aggregation to occur. However, it affects only the cmc (as shown by Eq. (1.5)) but not the equilibrium area a_e (as shown by Eq. (1.4)), which determines the size and shape of the aggregate. The second contribution, the free energy of residual contact between the aggregate core and water, is positive and decreases in magnitude as the area a decreases. A decrease in the area a corresponds to an increase in the aggregation number g for all aggregate shapes, as shown on Table 1.1. Hence, this contribution promotes the growth of the aggregate. The third contribution, the free energy due to headgroup repulsions, is also positive and increases in magnitude if the area a decreases or the aggregation number g increases. Hence, this contribution is responsible for limiting the growth of aggregates to a finite size. Thus, the Tanford model clearly identifies why aggregates form, why they grow, and why they do not keep growing but remain finite in size.

The Tanford model explicitly attributes a central role to the surfactant headgroup in controlling self-assembly. The magnitude of headgroup repulsions determines the equilibrium area per molecule, and hence the size and shape of the surfactant aggregate. In contrast, the surfactant tail does not affect the equilibrium area per molecule but influences only the magnitude of the cmc. We have shown earlier [21, 22] that although the surfactant tail does not affect the equilibrium area in the framework of Tanford model, there are other

implicit ways by which the tail does exert an influence on the aggregate size and shape. We describe four situations that demonstrate the implicit role of the tail in determining the aggregate size and shape, as follows

(i) *Spherical micelles from nonionic or zwitterionic surfactants.* Consider the formation of spherical micelles from a family of nonionic or zwitterionic surfactants with the same headgroup but differing tail lengths. The headgroup repulsion parameter α is a constant for the homologous family of molecules. Therefore, the equilibrium area a_e calculated from Eq. (1.4) is independent of the tail length, and the packing parameter $P = v_o/a_e\ell_o$ is also independent of the tail length (since v_o/ℓ_o does not change with tail length). Using the geometrical relations in Table 1.1, the aggregation number of the spherical micelles is given by

$$g = \frac{36\,\pi\,v_o^2}{a_e^3} \tag{1.6}$$

One may note that because of the proportionality of v_o to the number of carbon atoms n_C in an aliphatic tail and the tail length independence of a_e, the aggregation number g is proportional to n_C^2 or the square of the surfactant tail length. The tail does determine the actual size or aggregation number of the spherical micelle.

(ii) *Spherical micelles from ionic surfactants.* Consider a family of ionic surfactants, with the same headgroup but differing tail lengths. The implicit influence of the tail arises as follows. The equilibrium area a_e depends on the headgroup repulsion parameter α, which in this case accounts for electrostatic interactions between the ionic headgroups. The electrostatic interactions are influenced by the ionic strength of the solution through the inverse Debye length κ, which for uni-univalent ionic systems is given by

$$\kappa = \left[\frac{8\,\pi\,e^2 n_o}{\varepsilon\,kT}\right]^{1/2} = \left[\frac{8\,\pi\,e^2}{\varepsilon\,kT}\,\frac{cmc}{1000}\,N_{Avo}\right]^{1/2} \tag{1.7}$$

In Eq. (1.7), n_o is the number of counterions in solution per cm^3. In the absence of any added electrolyte, the ionic strength is determined primarily by the concentration of the singly dispersed surfactant in solution, which is practically equivalent to the cmc. The second equality in Eq. (1.7) represents this condition where n_o is related to the cmc in moles/liter, N_{Avo} is the Avogadro number and the factor 1000 converts concentration per liter to that per cm^3 of solution. The cmc is dependent on the transfer free energy of the tail, which directly depends on the length of the tail. Thus, the tail length implicitly influences the headgroup interaction parameter α, hence, the equilibrium area a_e, and the size of the micelles, for ionic surfactants. In the presence of significant amount of

added electrolyte, this tail length effect on the Debye length and the headgroup interactions diminishes and even disappears.

(iii) *Formation of cylindrical micelles.* Consider the formation of large spherocylindrical micelles of size g containing g_{cap} molecules in the two spherical endcaps and (g-g_{cap}) molecules in the middle cylindrical part. Eq. (1.1) for the size distribution of micelles can be rearranged to explicitly represent the molecules in the middle cylindrical domain and those in the endcap spherical domains. Based on this, the size distribution of aggregates and the average aggregation numbers are given [11, 21] by the expressions:

$$X_g = \frac{1}{K}\, Y^g, \quad Y = X_1 \exp\left(-\frac{\Delta\mu^o_{cyl}}{kT}\right), \quad \ln K = g_{cap}\left[\frac{\Delta\mu^o_{cap} - \Delta\mu^o_{cyl}}{kT}\right]$$

$$g_n = g_{cap} + [K\,(X_{tot} - X_1)]^{1/2}, \quad g_w = g_{cap} + 2[K\,(X_{tot} - X_1)]^{1/2} \quad (1.8)$$

In Eq. (1.8), $\Delta\mu^o_{cyl}$ and $\Delta\mu^o_{cap}$ are the changes in the standard chemical potentials when singly dispersed surfactant molecule becomes incorporated in the cylindrical middle and spherical endcaps, respectively, of the spherocylindrical aggregate. The variable K is a measure of the free energy cost of having g_{cap} molecules in the spherical endcaps compared to the energetically favored cylindrical middle. The parameter Y indicates the possibility of occurrence of cylindrical aggregates at a given concentration of the singly dispersed surfactant molecules. g_n and g_w denote the number and weight average aggregation numbers, respectively, calculated as a function of the total surfactant concentration X_{tot}.

The tail length of the surfactant determines g_{cap} since for increasing tail lengths, larger number of molecules could be accommodated in the endcaps. For single-tail amphiphiles, g_{cap} varies from 27 for C_8, 55 for C_{12} and 115 for C_{18} tails. Therefore, for a homologous family of surfactants, even when the equilibrium area per molecule remains independent of tail length, the parameter K would increase dramatically with increasing tail length. Therefore, the tail length significantly influences the size of the cylindrical micelles even for a constant equilibrium area per molecule. This also implies that even when the equilibrium area per molecule favors the formation of cylindrical micelles, we may observe only spherical or globular micelles when the tail length is short if K is not large enough.

(iv) *Formation of spherical bilayer vesicles.* Consider solution conditions that favor the formation of spherical bilayer vesicles. When bilayer vesicles form with an enclosed aqueous cavity, the headgroups of the surfactants in the inner layer of the bilayer are located within this aqueous cavity. Therefore, for bilayer vesicles to form, at a minimum, the volume per surfactant molecule of this inner aqueous cavity must be larger than the volume of the headgroup. Furthermore, the inner radius of the vesicle

will have to be larger than the length of the headgroup (in the direction normal to the hydrophobic surface).

Consider a vesicle whose hydrophobic domain has an outer radius R_o and the half-bilayer thickness is R. R is usually smaller than the extended length ℓ_o of the tail. The inner radius of the hydrophobic domain is thus $(R_o - 2R)$. Israelachvili et al. [11] have shown that R_o can be calculated from

$$R_o = \frac{R\left[3 + \sqrt{3\left(\frac{4v_o}{a_e R} - 1\right)}\right]}{6\left(1 - \frac{v_o}{a_e R}\right)} \tag{1.9}$$

If the number of surfactant molecules in the inner layer of the bilayer is g_i, then the volume per molecule of the aqueous cavity V_{cav} is given by

$$g_i = \frac{4\pi (R_o - 2R)^2}{a_e}, \quad V_{cav} = \frac{4\pi (R_o - 2R)^3}{3 g_i} = \frac{(R_o - 2R)\, a_e}{3} \tag{1.10}$$

It may be noted that in writing Eq. (1.10), we have assumed for simplicity that the equilibrium areas per molecule and the thicknesses of the layers are the same for the inner and the outer layers of the spherical bilayer vesicle. This assumption can be relaxed, but for the purposes of demonstrating the tail length effect, those additional details are not necessary. From Eq. (1.9) we note that for a homologous family of surfactants, with the equilibrium area a_e remaining the same, the outer vesicle radius R_o is roughly proportional to the tail length. From Eq. (1.10) we see that with decreasing chain length, the aqueous cavity volume per surfactant molecule (in the inner layer of the bilayer) decreases. Some illustrative calculations are presented in Table 1.2 for different values of the packing parameter P. In performing the calculations, for simplicity, we have assumed that the half bilayer thickness R of the vesicle is equal to the extended length ℓ_o of the surfactant tail. The calculations have been performed for a surfactant with two alkyl chains in the tail, taking $v_o/\ell_o = 0.42\ \text{nm}^2$.

For each packing parameter, the corresponding equilibrium area per molecule calculated as $a_e = (v_o/\ell_o)/P$, is also listed in Table 1.2. For alkyl chains having 8–18 carbon atoms, (n_C), the outer radius R_o of the vesicle is calculated using Eq. (1.9) and the aqueous cavity volume per molecule, V_{cav} is calculated using Eq. (1.10) and the results are summarized in Table 1.2. Therefore, for a homologous family of double-tailed surfactants with the unchanging equilibrium area per molecule (or constant packing parameter), the surfactants with longer tails may form vesicles, but as the tail length decreases, the cavity volume can become smaller than the volume necessary to accommodate the surfactant headgroup, thereby preventing the formation of the bilayer vesicle. Indeed, even when the packing parameter is above 1/2

Table 1.2 Tail length dependence of vesicle interior volume per molecule.[a)]

		$P = 0.75$ $a_e = 0.56\ nm^2$		$P = 0.80$ $a_e = 0.53\ nm^2$		$P = 0.90$ $a_e = 0.47\ nm^2$		$P = 0.95$ $a_e = 0.44\ nm^2$	
n_C	ℓ_o (nm)	R_o (nm)	V_{cav} (nm^3)	R_o (nm)	V_{cav} (nm^3)	R_o (nm)	V_{cav} (nm^3)	R_o (nm)	V_{cav} (nm^3)
8	1.15	4.17	0.348	5.3	0.531	11.1	1.368	22.6	2.992
10	1.4	5.08	0.423	6.5	0.647	13.5	1.666	27.5	3.643
12	1.65	5.99	0.499	7.7	0.762	15.9	1.963	32.4	4.293
14	1.9	6.90	0.575	8.8	0.878	18.3	2.261	37.3	4.944
16	2.15	7.80	0.650	10.0	0.943	20.7	2.558	42.2	5.594
18	2.4	8.71	0.726	11.1	1.109	23.2	2.856	47.2	6.245

a) Detailed computations of free energy minimizations allowing the half bilayer thicknesses of the inner and outer layers of the vesicle to be different and the areas per molecule at the inner and the outer surface to be different will give different predictions for the radius R_o and the cavity volume V_{cav}. But the qualitative result that the cavity volume decreases with decreasing tail length for any given packing parameter remains valid.

required for bilayers to form, bilayers may not form for surfactants of shorter tail lengths unless the packing parameter is large enough to accommodate the headgroups in the vesicle interior.

1.2.2 de Gennes Model for Block Copolymer Micelles

In contrast to the surfactant aggregates discussed above that are formed in water as the solvent, block copolymer micelles can be generated in any solvent as long as the solvent is nonselective to one block (solvophobic block denoted as A) and selective to the other block (solvophilic block denoted as B). The solvophobic block forms the core of the aggregate and the solvophilic block forms the shell or the corona of the aggregate (Figure 1.2).

de Gennes [16] analyzed the formation of AB diblock copolymer micelles in a selective solvent by minimizing the free energy per molecule of an isolated micelle ($\Delta\mu_g^o$). The micelle core was assumed to be fully segregated, devoid of any solvent, and the interface is treated as sharp. In the de Gennes model, the free energy of formation of the micellar core–corona interface and the free energy of stretching of the solvophobic block constituting the micelle core control the micellization behavior.

The free energy model of de Gennes can be written as

$$(\Delta\mu_g^o) = (\Delta\mu_g^o)_{A,Tr} + (\Delta\mu_g^o)_{A,def} + (\Delta\mu_g^o)_{Int}$$

$$(\Delta\mu_g^o) = (\Delta\mu_g^o)_{A,Tr} + \frac{R^2}{N_A} + \sigma\frac{N_A}{R} \tag{1.11}$$

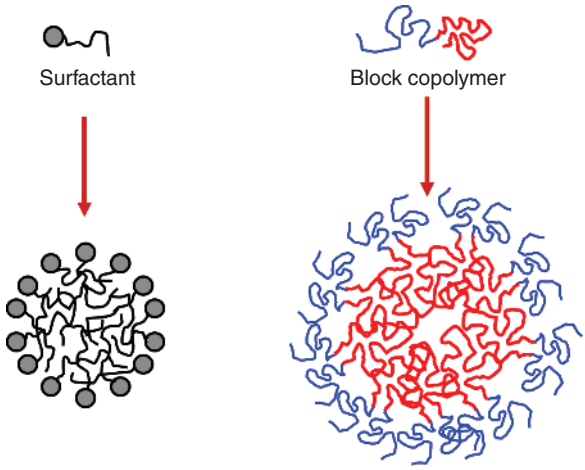

Figure 1.2 The formation of block copolymer micelle in a solvent selective to one of the blocks is analogous to the formation of the surfactant micelle. The solvophobic block of the block copolymer is equivalent to the surfactant tail while the solvophilic block of the block copolymer plays the role of surfactant headgroup.

The first term is the transfer of the solvophobic block A from the incompatible solvent to the micelle core resembling a melt of polymer block A. This term was not explicitly written in the original de Gennes paper but was obviously implied as it is the negative free energy contribution promoting self-assembly to occur. This is entirely analogous to the tail transfer free energy considered for surfactants. The second term is the stretching or elastic deformation of the solvophobic block A within the micelle core. The third term is the free energy of formation of the interface between the micelle core and the corona. The core block stretching is related to the core dimension R and the number of segments N_A in the A block while the interfacial free energy is related to the area per molecule a, which is inversely related to the core radius R. Explicit expressions for each of the contributions are also shown in Eq. (1.11) in the spirit of scaling models, excluding any numerical coefficients and treating all variables as nondimensional. In the last term accounting for the interfacial free energy, the relation between the area per molecule and core radius given in Table 1.1, $a \sim N_A/R$, has been used, noting that the volume of block A is proportional to the number of segments N_A in the block. From the minimization of the free energy, the de Gennes model predicts that the micelle core radius R and the aggregation number g are related to the size N_A of the solvophobic block as

$$R \sim N_A^{2/3}\sigma^{1/3}, \quad g \sim R^3/N_A \sim N_A\sigma \tag{1.12}$$

In the de Gennes free energy model, the solvophilic block B is considered to have no influence on the micelle characteristics and therefore the aggregate size has no dependence on the number of segments N_B in the B block. Note that the solvophilic block interactions in block copolymer micelles are analogous to the headgroup interactions in surfactant micelles. This offers a marked contrast to the Tanford model for surfactants, where the headgroup repulsions were the

principal contribution controlling the finite size of surfactant aggregates and the influence of the tail was not explicitly recognized.

1.2.3 Surfactant Self-Assembly Model Incorporating Tail Effects

The block copolymer micelle model treats the elastic stretching of the solvophobic block when micelle core comes into existence as a key contribution to the micelle free energy, but this is not considered in the Tanford model for surfactants. Therefore, we have introduced this as a new contribution in the free energy model for surfactant micelle [21, 22] by adopting the treatment pioneered by Semenov [23] for block copolymer chain stretching in confined geometries. The derivation of this expression takes into account the fact that the tail has to deform nonuniformly along its length to fill the aggregate core with uniform density.

The free energy model for surfactants, incorporating the contribution from tail packing (or elastic deformation), can be written as

$$\left(\frac{\Delta\mu_g^o}{kT}\right) = \left(\frac{\Delta\mu_g^o}{kT}\right)_{Tail} + \left(\frac{\Delta\mu_g^o}{kT}\right)_{Int} + \left(\frac{\Delta\mu_g^o}{kT}\right)_{Head} + \left(\frac{\Delta\mu_g^o}{kT}\right)_{Pack}$$

$$\left(\frac{\Delta\mu_g^o}{kT}\right)_{Pack} = \frac{3\pi^2}{80}\frac{R^2}{NL^2}, \quad \frac{5\pi^2}{80}\frac{R^2}{NL^2}, \quad \frac{10\pi^2}{80}\frac{R^2}{NL^2} \tag{1.13}$$

The first three free energy contributions come from the original Tanford model while the fourth contribution for packing is based on the tail stretching contribution viewed as a dominant factor in the block copolymer theory. The three expressions shown for packing free energy contributions correspond to spheres, cylinders, and planar bilayers, respectively. In the packing free energy contribution, L is a characteristic segment length that is taken to be 0.46 nm (see Ref. [21] for details) and N is the number of segments in a tail such that $N L = \ell_o$ and $N L^3 = v_o$. It should be mentioned that the treatment of Semenov focused on the arrangement of polymer segments in domains formed by high molecular weight block copolymers. In such a case, the dimension R would be typically much larger than the unperturbed end to end distance $N^{1/2}L$ of the polymer block, with N being in many 10s or 100s. Therefore, in developing the free energy model [23], the microscopic elastic energy was written considering only chain stretching. For classical single chain surfactants with 8–18 carbon atoms in the tail, the number of segments N is typically two to five and the direct application of the result from block copolymer analysis need not be quantitatively accurate. Nevertheless, because of the simplicity of this analytical expression and the alternative of computationally intensive estimation methods for this packing free energy contribution, we have applied this analytical equation for all of our predictive computations [21].

From geometrical relations for the aggregates, we have $R = 3\,v_o/a$, $2\,v_o/a$, and v_o/a for the three geometries (Table 1.1). Introducing these in Eq. (1.13), the

packing free energy contribution can be rewritten as

$$\left(\frac{\Delta\mu_g^o}{kT}\right)_{Pack} = \frac{Q}{a^2}, \quad Q_{sph} = \frac{27}{8}v_oL, \quad Q_{cyl} = \frac{20}{8}v_oL, \quad Q_{bilayer} = \frac{10}{8}v_oL, \tag{1.14}$$

where the symbol Q is used to denote the coefficient of $1/a^2$ in the free energy expression and it stands for Q_{sph}, Q_{cyl}, or $Q_{bilayer}$ depending upon the aggregate shape. The equilibrium area a_e given before by Eq. (1.4) is now obtained from the modified relation

$$\frac{\partial}{\partial a}\left(\frac{\Delta\mu_g^o}{kT}\right) = \left(\frac{\sigma}{kT}\right) - \left(\frac{\alpha}{kT}\right)\frac{1}{a^2} - \frac{2Q}{a^3} = 0, \quad at \quad a = a_e$$

$$a_e = \left(\frac{\alpha}{\sigma} + \frac{2Q/a_e}{\sigma/kT}\right)^{1/2} \tag{1.15}$$

Since the variable Q is dependent on the tail, the tail has direct influence over the equilibrium area a_e and the packing parameter P. From Eq. (1.15), we can see that the incorporation of the tail-packing effect causes an increase in the equilibrium area per molecule and correspondingly a decrease in the packing parameter, compared to the free energy model that neglects the tail-packing effect. The consequence is the direct control exerted by the tail over the size and shape of the equilibrium aggregate.

Illustrative numerical calculations have been carried out taking into account this packing free energy contribution. For this purpose, we have chosen a value of $(\alpha/kT) = 5\,\text{nm}^2$ for the headgroup interaction parameter and $(\sigma/kT) = 12\,\text{nm}^{-2}$, consistent with σ being around $50\,\text{mN m}^{-1}$ for aliphatic hydrocarbons-water interface. Q depends on the tail length as well as the shape of the aggregate within which the tails have to pack, as shown in Eq. (1.14). A summary of the calculated results for various tail lengths of single tail surfactant micelles is given in Table 1.3. Shown on the table are the equilibrium area a_e calculated from the Tanford model (Eq. (1.4)) and the model that explicitly considers tail packing (Eq. (1.15)) and takes into account the elastic deformation of the surfactant tail.

Since the Tanford model does not attribute any role for the surfactant tail in controlling the micelle size or shape, the calculated equilibrium area per molecule is independent of the tail length. In contrast, in the model that includes the hydrophobic tail stretching in the micelle core, the area per molecule shows a tail length dependence and increases as the tail length increases. All surfactants listed on the table form only spherical micelles. One can observe that the tail length influence is appreciable enough when it comes to considering the aggregation number of the spherical micelles.

Table 1.3 Influence of tail-packing free energy contribution on the size of spherical surfactant micelles.

		a_e (nm^2)	g	Q_{sph} (nm^4)	a_e (nm^2)	g
n_C	v_o (nm^3)	Based on Eq. (1.4)		Based on Eqs. (1.14) and (1.15)		
8	0.243	0.645	25	0.377	0.711	19
10	0.297	0.645	37	0.461	0.723	26
12	0.351	0.645	52	0.545	0.735	35
14	0.405	0.645	69	0.629	0.747	45
16	0.459	0.645	89	0.713	0.758	55

1.2.4 Star Polymer Model of Block Copolymer Self-Assembly Incorporating Headgroup Effects

The star polymer model for block copolymer micelles explicitly recognizes the role of the solvophilic block B. The star polymer model for micelles is built on the analogy between the conformation of star-shaped polymers and micelles. Star polymers resemble micelles, but for the important difference that a chemical link exists at the center between the various branches of the star polymer (Figure 1.3). Daoud and Cotton [24] studied the conformation of a uniform star polymer, with g branches joining at the origin, present in a good solvent. They identified three distinct regions in this conformation – a swollen region, an unswollen region, and a uniform density region. For each of these three regions, they developed expressions for the radial concentration profiles utilizing the concept of blobs employed in theories of semi-dilute solutions of linear polymers. They also derived an expression for the spatial extension of the branches as a function of the number of branches in the star polymer.

The results from the Daoud-Cotton model are the basis of the scaling analysis of spherical and cylindrical micelles in good and theta solvents, pioneered by Zhulina and Birshtein [25] and the star model for spherical micelles in good solvents independently formulated by Halperin [26]. We have applied the Daoud-Cotton results to formulate a star polymer model for both micellization as well as solubilization [27] in block copolymer solutions. The development of various free energy contributions and the predictions for different cases of block composition, block size, and solvent-block interactions are detailed in that study. Here, we will present only the final results from the star polymer model, focusing on the role of the soluble block. Therefore, the results are given only for the case when the selective solvent is a good or theta solvent for the solvophilic block B, since this is the condition where we expect

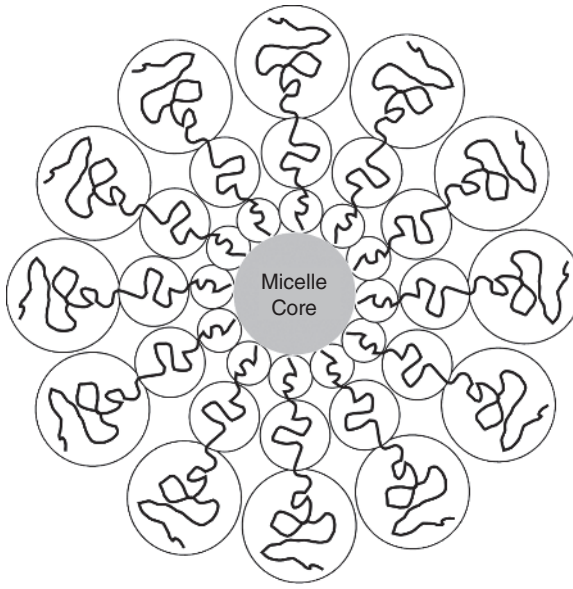

Figure 1.3 Schematic representation of the star polymer model of block copolymer micelle. The star is made up of multiple branches all connected to the surface of the micelle core. Each branch is made of a succession of blobs whose size increases radially outwards. The free energy is calculated as the number of blobs.

the solvophilic block interactions to be most important. As is conventional in scaling analysis, all numerical coefficients are ignored while writing various equations. All spatial variables such as the core radius R, the corona thickness D, and the core area per molecule a, are expressed as dimensionless quantities and the free energy contributions are expressed in units of kT.

Based on the application of the star polymer concept, the free energy per molecule of the block copolymer micelle is written as

$$(\Delta\mu_g^o) = (\Delta\mu_g^o)_{A,Tr} + (\Delta\mu_g^o)_{A,def} + (\Delta\mu_g^o)_{Int} + (\Delta\mu_g^o)_B$$

$$(\Delta\mu_g^o) = (\Delta\mu_g^o)_{A,Tr} + \frac{R^2}{N_A} + \sigma\frac{N_A}{R} + g^{1/2}K_B, \qquad K_B = \ln\left(1 + \frac{D}{R}\right) \tag{1.16}$$

Note that the free energy of transfer of the solvophobic block A from the incompatible solvent to the micelle core is usually not explicitly written but is obviously implied. This term provides the negative free energy contribution driving aggregate formation but is independent of the size and shape of the aggregate and therefore is not needed for any aggregate size and shape calculations. The core block elastic deformation term and the interfacial energy term are as in the de Gennes model. The only new addition is the B block dependent term, written here based on the blob picture of the star polymer model. We carry out free energy minimization for the limiting case when $(\Delta\mu_g^o)_B$ is dominant compared to $(\Delta\mu_g^o)_A$. When N_B is much larger than N_A, the shell block free energy contribution $(\Delta\mu_g^o)_B$ can be dominant compared to the core block free energy contribution $(\Delta\mu_g^o)_A$. One may note that when $N_B \gg N_A$, we have

correspondingly $D/R \gg 1$. In this case, if the solvent is a good solvent for the B block, we get

$$R \sim N_A^{3/5}\sigma^{2/5}K_B^{-2/5},\ g \sim N_A^{4/5}\sigma^{6/5}K_B^{-6/5},\quad D \sim N_A^{4/25}N_B^{3/5}\sigma^{6/25}\omega_B^{1/5}K_B^{-6/25}$$

$$K_B = \ln\left(1+\frac{D}{R}\right) \approx \ln(D/R) \approx \ln\left(N_A^{-\frac{11}{25}}\,N_B^{\frac{3}{5}}\,\sigma^{-\frac{4}{25}}\,\omega_B^{\frac{1}{5}}\,K_B^{\frac{4}{25}}\right) \approx \ln\left(N_A^{-\frac{11}{25}}\,N_B^{\frac{3}{5}}\right) \tag{1.17}$$

where $\omega_B = (1/2 - \chi_{BS})$ and χ_{BS} is the block B – solvent S Flory interaction parameter. If the solvent S is a theta solvent for the B block, we get:

$$R \sim N_A^{3/5}\sigma^{2/5}K_B^{-2/5},\ g \sim N_A^{4/5}\sigma^{6/5}K_B^{-6/5},\quad D \sim N_A^{1/5}N_B^{1/2}\sigma^{3/10}3K_B^{-3/10}$$

$$K_B = \ln\left(1+\frac{D}{R}\right) \approx \ln(D/R) \approx \ln\left(N_A^{-\frac{2}{5}}\,N_B^{\frac{1}{2}}\,\sigma^{-\frac{1}{10}}\,K_B^{\frac{4}{25}}\right) \approx \ln\left(N_A^{-\frac{2}{5}}\,N_B^{\frac{1}{2}}\right) \tag{1.18}$$

Note that we have the same relations for the core radius R and the micelle aggregation number g as in Eq. (1.17) but a different dependence for the corona thickness D depending on whether the solvent is a good solvent or a theta solvent for the B block. In both cases, we find the micelle core radius and aggregation number are only weekly influenced by the solvophilic block, with a logarithmic dependence on N_B (appearing through K_B). Certainly this is much weaker than the case of surfactant micelles, where the headgroup interactions are paramount.

1.2.5 Mean Field Model of Block Copolymer Self-Assembly Incorporating Headgroup Effects

The surfactant micelle model treats the repulsive interactions between the hydrophilic headgroups as a central contribution to the micelle free energy. Indeed, without this contribution finite micelles cannot be realized. In block copolymers, an analogous free energy contribution should arise from the difference in state of the hydrophilic block B when the singly dispersed copolymer becomes part of the micelle. However, this contribution is not considered in the free energy model of de Gennes. While the star polymer model considered the B block dependent free energy, it did not yield a significant dependence of the micelle core radius and aggregation number on the size N_B of the B block but only a weak logarithmic dependence because the core does not appear as a significant factor in the asymptotic star model that focuses mainly on the corona. Therefore, we have developed mean field models [28–31] of block copolymer micelles, explicitly accounting for the coronal region's contribution to the free energy of micellization. We have considered two alternate options.

In one option, we treat the corona to be of uniform solvent concentration and correspondingly the corona B block is nonuniformly stretched as described by Semenov [23]. Alternately, we treat the corona B block to be uniformly stretched as in the Flory model [32], and correspondingly the corona region has a radially varying solvent concentration profile. The free energy model of de Gennes (Eq. (1.5)) is now modified to include the osmotic (dilution term) and elastic (deformation term) free energy contributions associated with the B block, equivalent to the headgroup repulsions for surfactants.

The free energy model based on uniform concentration and nonuniform chain stretching in the corona region has the form

$$
\begin{aligned}
(\Delta\mu_g^o) &= (\Delta\mu_g^o)_{A,Tr} + (\Delta\mu_g^o)_{A,def} + (\Delta\mu_g^o)_{Int} + (\Delta\mu_g^o)_{B,dil} + (\Delta\mu_g^o)_{B,def} \\
\left(\frac{\Delta\mu_g^o}{kT}\right)_{A,def} &= q\,\frac{p\pi^2}{80}\,\frac{R^2}{(N_A/q)L^2} \\
\left(\frac{\Delta\mu_g^o}{kT}\right)_{Int} &= \frac{\sigma}{kT}\,a, \quad \sigma = \frac{kT}{L^2}\left(\frac{\chi_{AS}}{6}\right)^{1/2} \\
\left(\frac{\Delta\mu_g^o}{kT}\right)_{B,dil} &= N_B\left[\frac{\nu_B}{\nu_S}\frac{1-\varphi_B}{\varphi_B}\ln(1-\varphi_B) + \frac{\nu_B}{\nu_S}(1-\varphi_B)\,\chi_{BS}\right] \\
\left(\frac{\Delta\mu_g^o}{kT}\right)_{B,def} &= \frac{3}{2}\,\frac{L\,R}{\left(\frac{a}{q}\right)\varphi_B}\,P
\end{aligned}
\tag{1.19}
$$

Eq. (1.19) is written to be valid for AB diblock and symmetric BAB triblock copolymers, with $q = 1$ for AB diblock and $q = 2$ for BAB triblock copolymers. The first term is the free energy of transfer of the solvophobic block A from the incompatible solvent to the micelle core and it provides the negative free energy driving micelle formation to occur. The second term is the A block elastic deformation energy contribution with $p = 3$ for spheres, $p = 5$ for cylinders, and $p = 10$ for lamella. The A block deformation term is written based on the Semenov treatment that we had applied also to surfactant tails, as shown in Eq. (1.13). The third term is the interfacial energy term where the interfacial tension σ can be an experimentally measured value or it can be calculated based on the expression provided by Helfand [14], as shown. Here, the variable χ_{AS} denotes the Flory interaction parameter of the A block with solvent S and L is the characteristic segment size. The fourth term is the B block osmotic or dilution term. It is written using the formulation of Flory polymer solution thermodynamics. Here, χ_{BS} denotes the Flory interaction parameter of the B block with solvent S, L is the characteristic segment size, and φ_B is the volume fraction of polymer B segments in the corona region. The last term is the B block deformation term, also based on the approach developed by Semenov [23]. In this expression, $P = (D/R)/(1 + D/R)$ for spheres, $P = \ln(1 + D/R)$ for cylinders, and

Table 1.4 Geometrical relations for block copolymer aggregates.

Property	Sphere	Cylinder	Lamella
Core volume, V_C	$4\pi R^3/3$	πR^2	$2R$
Corona/Core volume ratio, V_S/V_C	$[(1+D/R)^3-1]$	$[(1+D/R)^2-1]$	$[(1+D/R)-1]$
Aggregation number, g		$V_C/(N_A v_A)$	
Core surface area/molecule, a	$3\,N_A v_A/R$	$2\,N_A v_A/R$	$N_A v_A/R$
Volume fraction of B in corona, φ_B	$(g\,N_B v_B)/V_S = (N_B v_B/N_A v_A)(V_C/V_S)$		

The symbols v_A and v_B refer to the molecular volumes of A and B segments, v_S is the molecular volume of the solvent, N_A and N_B are the number of segments of blocks A and B for both AB diblock and symmetric BAB triblock copolymers. The number of block copolymer molecules g in an aggregate, the aggregate core volume V_C, and the corona volume V_S all refer to the total quantities in the case of spherical aggregates, quantities per unit length in the case of cylindrical aggregates and quantities per unit area in the case of lamellar aggregates.

$P = (D/R)$ for lamellae [29, 30]. The Semenov treatment accounts for the fact that the chain deformation has to be nonuniform in order to maintain uniform concentrations of segments in the corona region. We note in passing that in our first model for block copolymer micelles [28], we had used the Flory model for chain elasticity that assumes uniform chain deformation to calculate the deformation free energy contribution, while also assuming the corona region to be uniform in concentration.

This free energy model is applicable to aggregates having spherical, cylindrical, and lamellar morphologies. All the geometrical properties of the aggregates appearing in the free energy expressions are summarized in Table 1.4. Note that in our detailed treatment of block copolymer micelles [28–30], we have also included a free energy contribution to account for the localization of the AB joint to a narrow volume of the aggregate and also a contribution that accounts for backfolding in the case of a BAB triblock copolymer. Both of these contributions are practically independent of the aggregate size and shape and therefore not shown in Eq. (1.19).

For illustrative purposes, calculations have been carried out for the PEO–PPO diblock copolymers aggregating in water, with water being a selective solvent for the PEO block and a poor solvent for the PPO block. One can expect the B block dependent free energy contribution to gain greater importance when the selective solvent changes from being a theta solvent to a good solvent for the B block. Our calculations for PEO–PPO block copolymer micelles considering uniform concentration in the corona and nonuniform chain stretching for the coronal B block (Semenov approach) yielded results summarized in Table 1.5. The predicted aggregate core radius R, corona thickness D, area per molecule at the core–corona interface a_e and the

Table 1.5 Model predictions of spherical micelles of PEO–PPO in water at 25 °C.

Block copolymer	R (nm)	D (nm)	a_e (nm^2)	g
$E_{34}P_{60}$	8.29	3.69	2.09	413
$E_{40}P_{70}$	9.02	4.21	2.25	455
$E_{26}P_{30}$	5.07	2.91	1.71	189
$E_{38}P_{43}$	6.16	3.95	2.02	235
$E_{54}P_{61}$	7.43	5.24	2.38	292
$E_{38}P_{29}$	4.48	3.81	1.88	134
$E_{48}P_{35}$	4.89	4.56	2.07	145
$E_{52}P_{40}$	5.33	4.89	2.17	164
$E_{74}P_{56}$	6.33	6.43	2.56	196
$E_{104}P_{35}$	3.93	7.27	2.58	75
$E_{122}P_{40}$	4.18	8.14	2.77	79
$E_{200}P_{64}$	5.27	11.6	3.52	99
$E_{154}P_{29}$	3.04	8.51	2.76	42
$E_{208}P_{39}$	3.53	10.6	3.20	49
$E_{236}P_{45}$	3.81	11.6	3.42	53
$E_{266}P_{50}$	4.00	12.6	3.62	56

aggregation number g for spherical micelles are listed for each of the diblock copolymer considered.

By correlating the predicted results, we find the following scaling relations for the PEO–PPO-water system:

$$R \sim N_A^{0.73} N_B^{-0.29}, \qquad g \sim N_A^{1.19} N_B^{-0.87}, \qquad D \sim N_A^{0.06} N_B^{0.60} \tag{1.20}$$

The core radius and the aggregation number show dependence on the solvophilic block B that was entirely absent in the case of de Gennes model and was much weaker in the case of the star polymer model. Indeed, the free energy contributions analogous to surfactant headgroup repulsions are very important for block copolymers and the contribution leads to stronger dependencies on the B block when the selective solvent is a very good solvent for the B block.

1.2.6 Tail Effects on Shape Transitions in Surfactant Aggregates

The rationalization of why surfactant molecules choose to self-assemble as spherical micelles, cylindrical micelles, or spherical bilayer vesicles and how one can cause a transition in shapes is a fundamental problem of interest.

In surfactant aggregates, since the hydrophobic domain is made up of the surfactant tails, irrespective of the shape of the aggregate, no point within the aggregate can be farther than ℓ_o from the aggregate-water interface, where ℓ_o is the extended length of the surfactant tail. In view of this constraint, and considering the geometrical properties of aggregates of different shapes, we have already referred to the well-known [11] connection between the molecular packing parameter and the aggregate shape: $0 \leq v_o/a\ell_o \leq 1/3$ for sphere, $1/3 \leq v_o/a\ell_o \leq 1/2$ for cylinder, and $1/2 \leq v_o/a\ell_o \leq 1$ for bilayer. Note that the free energy plays a fundamental role, as it should, in determining the magnitude of the packing parameter, because the equilibrium area per molecule a_e is obtained from the condition of minimum free energy. We have already discussed how tail packing contributes to the free energy, as described in Eq. (1.13). To assess the consequences of this contribution to determining the shape of the aggregate, we can compare the equilibrium areas predicted by the Tanford model (Eqs. (1.3) and (1.4)), which ignores this tail contribution against the modified model (Eqs. (1.13) and (1.15)) for illustrative cases where shape transitions may occur. The calculations have been performed for a surfactant with a dodecyl alkane tail [22] and the results are summarized in Table 1.6. As mentioned earlier, $(\sigma/kT) = 12\,\text{nm}^{-2}$, consistent with σ being around 50 mN/m for the aliphatic hydrocarbon-water interface. The headgroup interaction parameter α/kT is taken as a variable in the range 5.0–0.6 nm^2 to reflect the condition where the headgroup repulsions are decreased by adding salt to an ionic surfactant solution.

The inclusion of the tail-packing free energy (Eq. (1.15)) results in the equilibrium area a_e for surfactant aggregates being larger than that estimated from Eq. (1.3). Since in all cases the area per molecule is increased, the predicted packing parameter is always decreased when the tail-packing contribution is considered. Therefore, the predictions of equilibrium aggregate shapes are altered by the consideration of the tail elastic stretching. The calculated results show that when compared to the predictions of the Tanford model, accounting for the tail deformation results in larger spheres becoming smaller spheres at

Table 1.6 Predicted aggregate shape transitions for surfactant with dodecyl tail.

	a_e (nm^2)	$v_o/a_e\ell_o$	Shape	a_e (nm^2)	$v_o/a_e\ell_o$	Shape
α/kT (nm^2)	Based on Eqs. (1.3) and (1.4)			Based on Eqs. (1.13) and (1.15)		
5.0	0.645	0.326	Sphere	0.735	0.286	Sphere
3.0	0.500	0.42	Cylinder	0.629	0.333	Sphere
2.4	0.447	0.47	Large cylinder	0.565	0.372	Small cylinder
1.2	0.316	0.664	Bilayer	0.488	0.430	Cylinder
0.6	0.224	0.938	Large vesicle	0.374	0.561	Small vesicle

$\alpha/kT = 5.0\,nm^2$, spheres being preferred over cylinders at $\alpha/kT = 3.0\,nm^2$ and cylinders being preferred over bilayer for $\alpha/kT = 1.2\,nm^2$. It should be noted that in applying Eq. (1.15) for spherical bilayer vesicles, it would be necessary to allow for the inner and the outer layers of the vesicle to differ in their layer thicknesses and also the area per molecule at the inner and the outer surfaces to be different. Such refinements are essential for any predictive computations but for the limited purposes of demonstrating the influence of the tail, they are left out in Eq. (1.15) and the resulting computed results summarized in Table 1.6.

1.2.7 Headgroup Effects on Shape Transitions in Block Copolymer Aggregates

We have already seen how the solvophilic block free energy contributions (equivalent to the surfactant headgroup repulsions) significantly influences the size of spherical block copolymer micelles. The block copolymer aggregates also exist as cylinders or bilayers just as surfactant aggregates. The shape transitions have been examined for PEO–PPO diblock copolymers using the mean field model (Eq. (1.19)). The results obtained for spherical micelles was shown in Table 1.5 and the results for cylinders and lamella are given in Table 1.7.

From Tables 1.5 and 1.7, we note that for block copolymers that have similar hydrophobic block lengths ($EO_{16}PO_{50}$ and $EO_{266}PO_{50}$, or $EO_{12}PO_{35}$, $EO_{18}PO_{32}$, and $EO_{45}PO_{35}$, for example) aggregate shapes change from spheres at large PEO block size to cylinders and lamella as the block size of PEO decreases, clearly reflecting the solvophilic block (headgroup) effect on the equilibrium aggregate shapes. Further, for the block copolymers that have similar hydrophobic block lengths mentioned above, the core radius of the sphere is larger than the core radius of the cylinder, which, in turn, is larger than the half-bilayer

Table 1.7 Shapes of PEO–PPO diblock copolymer aggregates in water at 25 °C.[a)]

Block copolymer	R (nm)	D (nm)	a_e (nm^2)	g	Shape
$E_{12}P_{35}$	2.62	1.73	1.29	1.55	Lamella
$E_{12}P_{38}$	2.80	1.72	1.31	1.53	Lamella
$E_{16}P_{50}$	3.26	2.19	1.48	1.35	Lamella
$E_{22}P_{69}$	3.90	2.85	1.71	1.17	Lamella
$E_{18}P_{32}$	4.02	2.27	1.54	16.5	Cylinder

a) The aggregation number g is defined as the number of molecules per nm length in the case of cylinder and the number of molecules per nm^2 area in the case of lamella.

Table 1.8 Predicted aggregate shapes for PEO–PPO–PPO triblock copolymer.[a)]

Trade name	Block copolymer	R (nm)	D (nm)	a_e (nm^2)	g	Aggregate shape
L62	$E_6P_{35}E_6$	1.75	0.96	1.93	1.04	Lamella
L72	$E_6P_{38}E_6$	1.87	0.96	1.96	1.02	Lamella
L92	$E_8P_{50}E_8$	2.19	1.22	2.20	0.91	Lamella
L122	$E_{11}P_{69}E_{11}$	2.65	1.60	2.52	0.80	Lamella
L63	$E_9P_{32}E_9$	1.45	1.39	2.13	0.94	Lamella
P103	$E_{17}P_{60}E_{17}$	3.87	2.17	2.99	8.1	Cylinder
P123	$E_{20}P_{70}E_{20}$	4.21	2.48	3.21	8.3	Cylinder
L64	$E_{13}P_{30}E_{13}$	3.42	1.64	2.54	58	Sphere
P84	$E_{19}P_{43}E_{19}$	4.19	2.24	2.97	74	Sphere
P104	$E_{27}P_{61}E_{27}$	5.09	2.99	3.47	94	Sphere
P65	$E_{19}P_{29}E_{19}$	3.06	2.18	2.74	43	Sphere
P75	$E_{24}P_{35}E_{24}$	3.36	2.63	3.02	47	Sphere
P85	$E_{26}P_{40}E_{26}$	3.66	2.82	3.16	53	Sphere
P105	$E_{37}P_{56}E_{37}$	4.38	3.73	3.70	65	Sphere
F77	$E_{52}P_{35}E_{52}$	2.75	4.31	3.69	26	Sphere
F87	$E_{61}P_{40}E_{61}$	2.92	4.84	3.96	27	Sphere
F127	$E_{100}P_{64}E_{100}$	3.70	6.98	5.00	35	Sphere
F68	$E_{77}P_{29}E_{77}$	2.13	5.13	3.94	15	Sphere
F88	$E_{104}P_{39}E_{104}$	2.48	6.39	4.55	17	Sphere
F98	$E_{118}P_{45}E_{118}$	2.67	7.03	4.86	18	Sphere
F108	$E_{133}P_{50}E_{133}$	2.83	7.66	5.14	20	Sphere

a) The aggregation number g is defined as the number of molecules per nm length in the case of cylinder and the number of molecules per nm^2 area in the case of lamella.

thickness of the bilayer. This prediction is the direct result of the chain elastic deformation free energy contribution. The shape transitions have also been explored for the commercially available triblock copolymers PEO–PPO–PEO of various molecular weights and block compositions and the results are summarized in Table 1.8.

The shape transition of block copolymer aggregates as a function of the block copolymer composition shown on Table 1.8 follows the behavior exhibited by surfactant aggregates as a function of headgroup repulsions. For surfactants, when the headgroup repulsions are weak, lamellar aggregates are favored while for strong headgroup repulsions, spherical micelles are formed. Cylindrical micelles result for intermediate values of headgroup repulsions. For the block copolymer aggregates, the free energy contributions associated with the

hydrophilic block B are analogous to the headgroup repulsions in surfactant micelles. Therefore, the pattern of aggregation observed for increasing headgroup repulsions in surfactants is exactly reproduced with increasing size of the hydrophilic block B in the case of block copolymers.

For surfactants, the packing parameter $P = v_o/a_e\ell_o$ provided the bounds for various aggregate shapes. Although the free energy determines the equilibrium area $a_{e,}$ the constraint that the radius of spherical or cylindrical micelle or half bilayer thickness cannot exceed ℓ_o plays a critical role in influencing the shape transitions. For example, a surfactant with a dodecyl tail can accommodate only 54 or fewer molecules if the aggregate shape is to remain spherical. However, in the case of the block copolymer, there is no equivalent constraint imposed by the extended length of the hydrophobic block since typically the block sizes are large. For example, if we look at the family of diblock copolymers in Table 1.5 with approximately 35 PO units, the extended length of the hydrophobic PPO block can be estimated roughly to be 16.1 nm, taking the segment length to be about 0.46 nm [33]. Corresponding to this extended length, spherical aggregates having a PO_{35} core block can accommodate as many as 5175 molecules. However the calculations show that we form spherical micelles of core radius 4.9 nm and aggregation number 145 for $EO_{48}PO_{35}$. When the PEO chain length is decreased, keeping the same hydrophobic block, even though there are no packing constraints that would prevent the sphere from growing from 145 molecules all the way up to 5175 molecules, the micelle does not grow retaining spherical shape but changes to a cylinder for $EO_{18}PO_{32}$ and bilayer for $EO_{12}PO_{35}$ (Table 1.7). This is a consequence of the free energy control over shape transitions. The predicted core radii are only 2.6, 4.0, and 4.9 nm for $EO_{12}PO_{35}$, $EO_{18}PO_{32}$, and $EO_{48}PO_{35}$ block copolymers forming lamellar, cylindrical, and spherical aggregates, much smaller than the extended length of 16.1 nm for the PPO block.

1.3 Self-Assembly of Nonclassical Amphiphiles Based on Head–Tail Competition

Over the last decade, there have been extensive studies on nonclassical amphiphiles that combine biological or inorganic elements or nanoparticles into classical surfactant, lipid, or polymer structures [34–48]. This book presents the most recent advances in these areas by pioneering scientists in these fields. Here, we present a few examples where the authors have invoked the application of existing theoretical models and the packing parameter concept to rationalize the observed self-assembly behavior. In all cases, the interactions involving the headgroups and the tail groups and the head-tail competition can be used to explain the patterns of aggregation observed.

1.3.1 Dendritic Amphiphiles

Dendritic polymers have a high degree of branching and therefore multiple number of end groups. These end groups can be readily modified by different functional groups such as reactive ligands, targeting moieties, etc., allowing for the possibility of multivalent binding interactions and enabling the practical applications of these molecules including for nanomedicine. This has generated significant interest in the design of amphiphiles built with dendritic polymers as the headgroups. An example is the series of dendritic amphiphiles synthesized in the Haag lab [34] involving glycerol-based generation 2 (G2) and generation 3 (G3) dendrons as hydrophilic headgroups and dialkyl chains as the tailgroup (Figure 1.4). They created six distinct dendritic amphiphiles by varying the generation of the headgroup and the length and geometry of the hydrophobic tailgroup.

The size distribution of the self-assembled structures were measured using dynamic light scattering (DLS) and the aggregate morphologies were observed

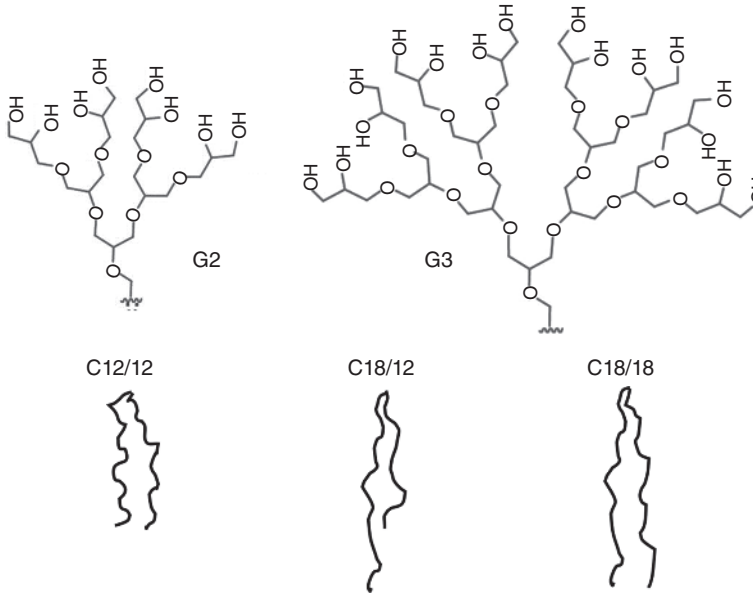

Figure 1.4 Headgroups and tailgroups of dendritic amphiphiles. The headgroups G2 and G3 are second- and third-generation dendrimers with hydroxyl surface groups. The tails are dialkyl chains with symmetric lengths of 12 and 18 carbon atoms for two molecules and asymmetric lengths of 12 and 18 carbon atoms for the third molecule, as shown in the figure. By combining these headgroups and tailgroups, six amphiphile structures were generated by the Haag lab [34]. They are depicted as G2C12/12, G2C12/18, G2C18/18, G3C12/12, G3C12/18, and G3C18/18.

using cryo-transmission electron microscopy (cryo-TEM). The DLS data predicted the existence of small micelles for all G3 amphiphiles (G3C12/12, G3C12/18, and G3C18/18) and the narrow intensity distributions indicated that the micelles were monodisperse. In contrast, the G2 amphiphiles revealed cylindrical aggregates of a markedly larger size by DLS, with the size distributions being wider and the average sizes considerably different for the three molecules considered. Cryo-TEM showed that for the symmetric G2 amphiphiles (G2C12/12 and G2C18/18), increasing the alkyl chain length from 12 to 18 led to a morphological transition from wormlike micelles to vesicles. However, the dissymmetric amphiphile G2C12/18 formed coexisting spherical as well as wormlike micelles reflected in the bimodal distribution obtained from light scattering.

The free energy model for classical surfactants (Eq. (1.13)) can be applied here. Because the dendritic amphiphiles considered are nonionic, the headgroup interactions are due only to steric repulsions. Based on the volumes and lengths of aliphatic hydrocarbon chains [21], the ratio v_o/ℓ_o is equal to 0.42 nm^2 for the C12/12 and C18/18 tails and is 0.35 nm^2 for the C12/18 tail. For the G2 dendritic amphiphile with 8 hydroxyl groups on the surface, the headgroup volume can be roughly estimated using group contributions to be about half of that for the G3 headgroup with 16 hydroxyl groups, implying that the headgroup interactions should be larger in magnitude for the G3 amphiphiles compared to the G2 amphiphiles. For illustrative purposes, taking the headgroup repulsion parameter $\alpha/kT = 5$ and 10 nm^2, to represent the G2 and G3 headgroups, the areas per molecule are calculated using Eqs. (1.14) and (1.15) for each of the three aggregate shapes. In calculating the area corresponding to a given shape, the chain packing free energy corresponding to that shape is used. If the results show that the packing parameter calculated assuming the spherical shape is above 1/3, then that solution is invalid. Similarly, if the packing parameter calculated assuming the cylindrical shape is greater than 1/2, then that solution is invalid. The calculated results are summarized in Table 1.9.

For the G2 amphiphiles, the packing parameter corresponds to a bilayer for both G2C12/12 and G2C18/18. Fort G2C18/18, the tail length is long enough and the aqueous cavity volume of the vesicle is large enough to accommodate the headgroups and vesicles can form. However, because the tail length is shorter for G2C12/12, the aqueous cavity volume is small to accommodate the headgroups and vesicle formation is prevented. In this case cylindrical micelles corresponding to $P = 1/2$ will form. For G2C12/18, cylindrical micelles are predicted because of the smaller v_o/ℓ_o. For the G3 amphiphiles, because the headgroup repulsion parameter is large, the area per molecule is larger and the packing parameter is smaller. In all three cases the packing parameter is larger than but close enough to 1/3 and therefore, globular micelles not much large than the largest spherical micelles are predicted. The calculations based on the free energy expression (Eq. (1.13)) is only illustrative and detailed predictive

Table 1.9 Aggregation behavior of dendritic amphiphiles.

	a_e (nm^2) from Eqs. (1.14) and (1.15)			$P = v_o/a_e\ell_o$		
Molecule	Sphere	Cylinder	Bilayer	Sphere	Cylinder	Bilayer
G2C12/12	0.803	0.769	0.715	0.523 invalid	0.546 invalid	0.587
G2C12/18	0.828	0.791	0.728	0.423 invalid	0.442	0.481 invalid
G2C18/18	0.855	0.812	0.741	0.491 invalid	0.517 invalid	0.567
G3C12/12	1.006	0.985	0.951	0.417 invalid	0.426	0.441 invalid
G3C12/18	1.025	0.997	0.959	0.341 invalid	0.351	0.365 invalid
G3C18/18	1.043	1.015	0.966	0.403 invalid	0.414	0.435 invalid

calculations would require quantitative modeling of the headgroup repulsions as we have done in our earlier work [21] and not the use of the phenomenological parameter α appearing in the Tanford free energy expression.

1.3.2 DNA Amphiphiles

DNA can be attached to hydrophobic polymers or lipids to provide DNA-polymer or DNA-lipid conjugates with amphiphilic properties [35–37]. The DNA not only serves as the hydrophilic portion of the amphiphile but can also be used to manipulate the self-assembly taking advantage of the DNA hybridization properties. Here, we discuss an example of DNA amphiphiles based on the work conducted in the Gianneschi laboratory [35] where they showed that short oligonucleotide conjugated lipids spontaneously assemble into unilamellar vesicles that can undergo reversible, vesicle-to-micelle transitions in response to specific DNA manipulations.

The system demonstrated by Thompson et al. [35] involves a DNA amphiphile that consist of two C_{18} alkyl hydrophobic tails, linked covalently to the 5′-termini of a 9-mer single-stranded ssDNA oligonucleotide (Lipid-DNA1 in Figure 1.5). This DNA amphiphile was found to self-assemble into uniformly shaped, spherical vesicles approximately 500 nm in diameter as characterized by multiple techniques. The unilamellar bilayer architecture of these vesicle assemblies was confirmed by cryoTEM with bilayer thicknesses of 8–9 nm, roughly equivalent to double the extended length of the DNA amphiphile. The vesicles were mixed with partially complementary 19-base ssDNA sequences

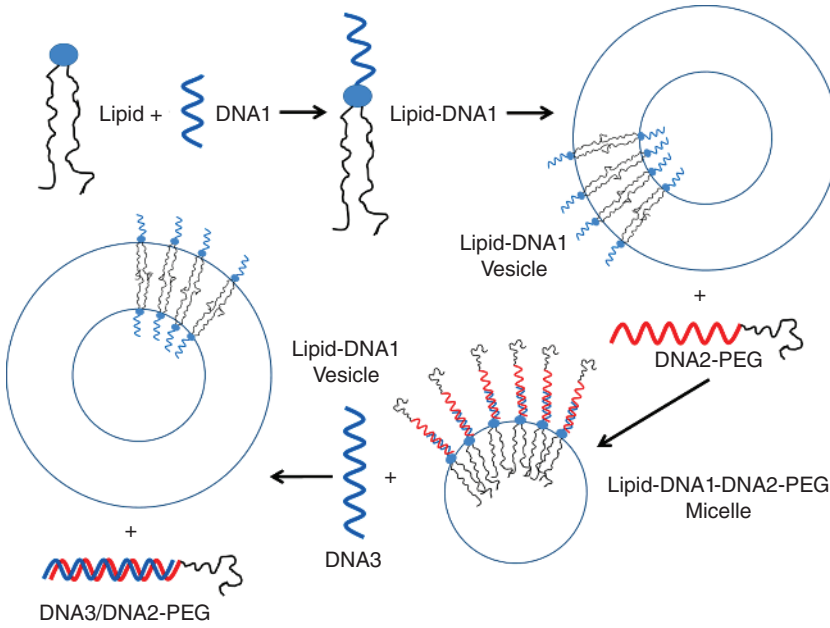

Figure 1.5 Use of DNA-programming to manipulate aggregate structures formed DNA amphiphiles [35]. The DNA1-lipid self assembles to form spherical unilamellar vesicles. The vesicles are then mixed with DNA2-PEG, which is partially complementary to DNA1. The complexation of DNA2-PEG with the DNA1 headgroups effectively creates a new headgroup, introducing additional steric and electrostatic repulsions between headgroups. This makes the vesical structure less optimal compared to spherical micelles and therefore the vesicle transform into micelles. These micelles are now mixed with DNA3, which is perfectly complementary to DNA2. Since DNA2-DNA3 binding is stronger than the DNA1-DNA2 binding, the DNA2-PEG is released from the micelles to form DNA3-DNA2-PEG hybrids. The headgroup of the amphiphile now reverts to DNA1 and the corresponding reduction in the headgroup repulsions makes the vesicle structure to be optimal allowing vesicles to reversibly reform from the spherical micelles. Extensive discussions on DNA containing amphiphiles are presented by Thompson and Gianneschi in Chapter 5 of this book.

modified at their 5′-termini with two 18-member ethylene glycol phosphoramidites (DNA2-PEG in Figure 1.5). The complexation of DNA2-PEG with DNA1 creates a new headgroup, which gives rise to a change in the structure of the aggregates from vesicles to micelles of about 20–25 nm in size. The spherical micelles were then combined with DNA3, which is a 19-base ssDNA strand perfectly complementary to DNA2. The hybridization of DNA2 with DNA3 being much stronger than the partial hybridization of DNA1 with DNA2, the DNA2-PEG was completely removed from the micelles, resulting in the reversible formation of vesicles of DNA1-lipid along with the formation of the stable 19-base pair duplex, DNA2-DNA3.

Considering DNA1-lipid, the DNA1 headgroup has negative charges from its phosphate groups but the net charge is always smaller than the number of phosphate groups. Therefore, the headgroup repulsions involve both electrostatic and steric interactions. The solution experiments were conducted in 20 or 50 mM Tris buffer and also in the presence of various amounts of $MgCl_2$. The presence of these electrolytes would decrease the extent of electrostatic interactions. Further, since the charges on the phosphate ions are located at some significant distance away from the hydrophobic core surface, the magnitude of electrostatic interactions would be further smaller. As a result, the headgroup repulsion parameter α/kT can be taken to be a small value. Taking, for example, $\alpha/kT = 3.0\,\text{nm}^2$, the equilibrium area calculated from Eq. (1.15) will be $0.63\,\text{nm}^2$ and the corresponding packing parameter P is 0.67, denoting the formation of a vesicle. When PEG-DNA2 complexes with the DNA1-lipid, the new headgroup is the DNA1-PEG-DNA2 complex. For this new headgroup, there would be some small increase in the electrostatic interactions and significant increase in the steric repulsions because of the large PEG group present. Taking, for example, a larger value of $\alpha/kT = 12.0\,\text{nm}^2$, the equilibrium area calculated from Eq. (1.15) will be $1.11\,\text{nm}^2$ and the corresponding packing parameter P is 0.378, implying a globular micelle, not much larger than the largest spherical micelle. Subsequently, on contact with DNA3 if all of the DNA2-PEG is removed by complete hybridization, we are left with DNA1 as the headgroup of the amphiphile, resulting in the reversible formation of vesicles. As mentioned previously, quantitative predictions would require more detailed modeling of the vesicle, allowing for the inner and the outer surfaces to be different and also modeling more precisely for the nature of headgroup repulsions.

1.3.3 Peptide Amphiphiles

Another class of nonclassical amphiphiles is that incorporating peptides such as for example, a molecule with hydrophobic polymer as the tail and a hydrophilic peptide with one or more hydrophilic amino acids as the headgroup [38–40]. Alternately, the hydrophobic tail could be an alkyl chain or a peptide itself composed of hydrophobic amino acids. Such peptide amphiphiles have been investigated in view of potential applications in nanomedicine. For example, the peptides can be selected to be substrates for cancer-associated proteins and thus amenable to proteolysis. Each peptide in the headgroup can be chemically modified by proteolysis by a specific enzyme, allowing for an enzyme-responsive switching of the morphology of the micelles used as drug delivery vehicles or as *in vivo* sensors [40]. Tirrell et al. investigated [38] peptide amphiphiles that form wormlike micelles resembling nanofibers, which are viewed as potential synthetic extracellular matrix materials for tissue engineering and regenerative medicine. The amphiphilic peptides are also being evaluated for materials design applications involving biomimetic

mineralization. The self-assembled peptide amphiphiles act as templates to induce nucleation, growth, and alignment of nanocrystals, thereby resulting in the formation of metallic nanowires and other highly ordered superstructures of minerals or composites.

Here we consider as an example studies on a series of amphiphilic peptides that were synthesized by Xu et al. [39]. In these amphiphiles, one lysine residue at the C terminus acts as the hydrophilic head and a chain of three to nine alanine residues serves as the hydrophobic tail. The C terminus was amidated, and the N terminus was acetylated, thus generating one positive charge per molecule (from the lysine residue side chain) at neutral pH. The molecular structures of the three amphiphiles denoted as A_3K, A_6K, and A_9K are shown on Figure 1.6.

The self-assembly of these peptide amphiphiles in aqueous solution has been examined by atomic force microscopy (AFM) and transmission electron microscopy (TEM). These studies have revealed that bilayer sheets were formed from A_3K, long wormlike micelles were formed from A_6K, and short nanorods were formed from A_9K. All of these peptide nanostructures were produced in solutions at a pH of about 6.0 when the lysine can have one positive charge. When the solution pH was changed to above 11, no characteristic supramolecular structures were formed, but instead irregular aggregates were

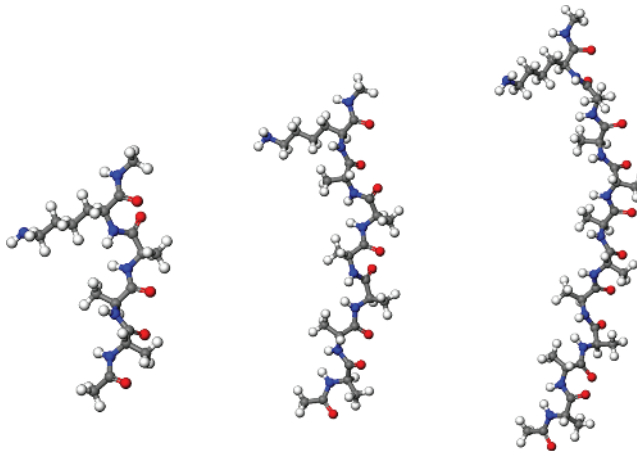

Figure 1.6 Molecular structures of A3K, A6K, and A9K amphiphilic peptides composed of multiple units of alanine as the hydrophobic part and a terminal lysine with one positive charge as the cationic hydrophilic part. Peptide amphiphiles with peptides as headgroups connected to a hydrophobic alkyl chain are extensively discussed by Leon and Tirrell in Chapter 6 of this book, focusing on unique peptide–peptide interactions and various aggregate structures that can result from it.

observed by TEM. Since the side chain amino group of lysine has a pKa of around 10, at pH 11, the headgroups became deprotonated, losing their charge and thereby changing the amphiphilic peptide to a hydrophobic molecule that simply precipitates in solution.

In the framework of the free energy model given by Eqs. (1.13)–(1.15), let us assume that for the appropriate headgroup parameter α/kT, the equilibrium area and the resulting packing parameter for A_3K correspond to a bilayer. Based on the free energy model, if the hydrophobic tail length is increased, the area per molecule would increase and the packing parameter would decrease in magnitude. This would qualitatively rationalize why for A_6K and A_9K cylindrical micelles are favored. Again, for A_6K the packing parameter would be larger than that for the A_9K amphiphile, implying that the A_6K can form long worm-like micelles while A_9K forms somewhat smaller cylindrical micelles. It should be noted, however, that the chain length effect modeled in Eqs. (1.13)–(1.15) is based on polymers with segments as basic units. The molecular structure and chain conformation for the peptides are significantly different from those of a polymer, and one would have to rederive an appropriate packing free energy contribution for these cases before any quantitative predictions can be made.

1.3.4 Protein–Polymer Conjugates

Protein–polymer conjugates combine natural biological molecules like polypeptides or proteins with synthetic polymer molecules to generate synergistic benefits from the presence of both components [41]. Many applications of polymer–protein conjugates are found in the area of therapeutics using the conjugates to construct targeted drug delivery vehicles. Because of conjugation with the polymer, the effective size of the protein is increased and its renal excretion rate decreased. The polymer chains also increase the half-life of the protein in the circulation system by protecting the protein from enzymatic degradation or removal by receptor recognition or complexation with antibodies. The attachment of the polymer to the protein also decreases the propensity of the protein to aggregate. One can also take advantage of the responsive characteristics of the polymer to generate stimuli-responsive protein function. In Figure 1.7, a number of polymer–protein conjugate types are schematically depicted incorporating homopolymers or block copolymers.

The polymer–protein conjugates can self-assemble into aggregates similar to the behavior exhibited by surfactants and block copolymers. Schematic of aggregates that can form from the polymer–protein conjugates are illustrated in Figure 1.8 assuming spherical shapes. Obviously, other shapes are also possible based on which of the shape-dependent free energies is the smallest and also the geometrical packing constraints applicable to the systems. Figure 1.7a depicts a hydrophobic homopolymer connected to the protein. In this case, self-assembly is possible if the protein is hydrophilic and plays the

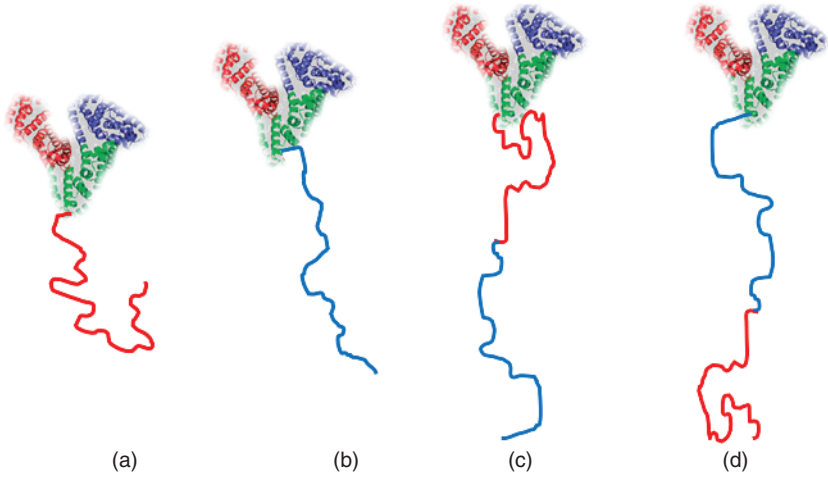

Figure 1.7 Schematic representations of protein–polymer conjugates. In (a), the protein is conjugated to a hydrophobic polymer chain while in (b), The protein is conjugated to a hydrophilic polymer chain. In (c) the protein is conjugated to the hydrophobic block of a diblock copolymer while in (d), the protein is conjugated to the hydrophilic block of a diblock copolymer.

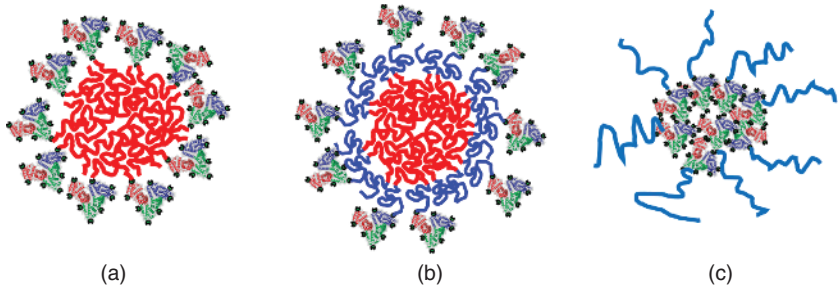

Figure 1.8 Schematic of spherical micelles anticipated from different protein–polymer conjugates. In (a), the hydrophobic polymer forms the core of the micelle while the hydrophilic protein forms the corona of the micelle. In (b), the hydrophobic block of the block copolymer controls micellization and the hydrophilic block and the hydrophilic protein conjugated to it are in the coronal region. If the protein is hydrophobic, other aggregation patterns could result for this molecule. In (c), the protein is hydrophobic and forms a core of protein molecules surrounded by the hydrophilic polymer conjugated to it. Such hydrophobic protein–polymer conjugates are discussed in detail by Olsen in Chapter 7 of this book.

role of the headgroup. Possible spherical micelle resulting from this conjugate is shown on Figure 1.8a. Figure 1.7b shows a hydrophilic homopolymer conjugated to a protein. In this case, self-assembly is possible provided the protein is hydrophobic. The resulting aggregate in spherical shape is shown on Figure 1.8c. Figures 1.7c,d show the protein conjugated to a diblock copolymer, either at the hydrophobic block end or at the hydrophilic block end. In this case, the block copolymers themselves are capable of forming aggregates, the presence of the protein can play the role of strengthening or weakening the aggregate depending on its hydrophilicity/hydrophobicity characteristics.

Depending on the nature of the protein, additional interactions should be considered while developing an expression for the free energy of aggregation. For example, in Figure 1.7a, the protein is connected to a hydrophobic homopolymer. The structure of a spherical micelle formed from such protein–polymer conjugate is depicted in Figure 1.8a. One can calculate the free energy of formation of aggregates for this system using Eq. (1.19) by introducing both steric and ionic repulsions between the protein molecules in the corona region of the micelle to represent the headgroup repulsions.

$$\left(\frac{\Delta\mu_g^o}{kT}\right) = \left(\frac{\Delta\mu_g^o}{kT}\right)_{A,Tr} + \left(\frac{\Delta\mu_g^o}{kT}\right)_{A,def} + \left(\frac{\Delta\mu_g^o}{kT}\right)_{Int} + \left(\frac{\Delta\mu_g^o}{kT}\right)_{Head}$$

$$\left(\frac{\Delta\mu_g^o}{kT}\right)_{Head} = \left(\frac{\Delta\mu_g^o}{kT}\right)_{Steric} + \left(\frac{\Delta\mu_g^o}{kT}\right)_{Ionic}$$

$$\left(\frac{\Delta\mu_g^o}{kT}\right)_{Head} = -\ln\left(1 - \frac{\nu_H}{a\delta}\right) + \frac{2\pi Z^2 e^2}{\epsilon a \kappa kT} \tag{1.21}$$

Equation (1.21) presents the simplest representation of the headgroup repulsions. The headgroup repulsion term α/a introduced by Tanford is now replaced by the first term denoting steric interactions represented by the van der Waals excluded volume model and the second term denoting ionic interactions represented by the Debye model [21]. Here ν_H is the volume of the protein headgroup present in the unit volume $a\delta$ of the corona region, a being the area per molecule and δ denoting the thickness of the corona. Z is the net charge on the protein, e is the electronic charge, and κ is the inverse Debye length that accounts for any counterions and added electrolytes.

For modeling the self-assembly of the hydrophobic protein-hydrophilic homopolymer conjugate shown on Figure 1.7b, one would have to introduce attractive interactions between the proteins. One can adapt Eq. (1.19) for this case recognizing that the proteins act as the equivalent of the tail group A.

$$(\Delta\mu_g^o) = (\Delta\mu_g^o)_A + (\Delta\mu_g^o)_{Int} + (\Delta\mu_g^o)_{B,dil} + (\Delta\mu_g^o)_{B,def}$$

$$\left(\frac{\Delta\mu_g^o}{kT}\right)_A = -S_H \frac{\sigma}{kT}$$

$$\left(\frac{\Delta\mu_g^o}{kT}\right)_{int} = \frac{\sigma}{kT}\,a \tag{1.22}$$

$$\left(\frac{\Delta\mu_g^o}{kT}\right)_{B,dil} = N_B\left[\frac{\nu_B}{\nu_S}\frac{1-\varphi_B}{\varphi_B}\ln(1-\varphi_B) + \frac{\nu_B}{\nu_S}(1-\varphi_B)\,\chi_{BS}\right]$$

$$\left(\frac{\Delta\mu_g^o}{kT}\right)_{B,def} = \frac{3}{2}\frac{L\,R}{a\,\varphi_B}\,P$$

In Eq. (1.22), S_H is the solvent accessible surface area of the protein molecule and the attractive protein interactions term is simply represented as the product of this surface area and a characteristic interfacial tension σ between the hydrophobic protein and the solvent water. The negative sign denotes that the interactions are attractive and provide the driving force for the self-assembly. All the remaining terms are as defined in Eq. (1.19) for the block copolymer self-assembly.

For the protein-block copolymer conjugates shown in Figures 1.7c,d, we have various possible aggregation patterns depending on whether the protein is hydrophilic or hydrophobic. If the protein is hydrophilic, the conjugate in Figure 1.7c can be simply treated like a triblock copolymer with a hydrophobic middle block and hydrophilic end blocks. The corona region in this case would consist of both the hydrophilic block of the copolymer and the protein. The conjugate in Figure 1.7d can be treated as a simple diblock copolymer by adding the additional headgroup repulsions term appearing in Eq. (1.21). On the other hand, if the protein is hydrophobic, then the conjugate in Figure 1.7c can be treated as a diblock copolymer, simply by adding the hydrophobic proteins contribution as represented in Eq. (1.22). The conjugate in Figure 1.7d can be represented as a triblock copolymer with end hydrophobic blocks and a middle hydrophilic block. The core now consists of a mixture of the hydrophobic block of the copolymer and the protein. Detailed quantitative models are not presented here but can be developed as described in this chapter and compared against aggregate structural data from systematic experiments with various polymers and proteins if they become available.

1.3.5 Amphiphilic Nanoparticles

An important class of nonclassical amphiphiles that is generating significant interest is that incorporating nanoparticles as a part of the amphiphile [42–48]. One example is an amphiphile containing a purely inorganic multinuclear headgroup of the polytungstate type R-$[PW_{11}O_{39}]_3$ [42], where R is the hydrophobic tail. Such polyoxometalate (POM) amphiphiles self-assemble into micelles and at higher concentrations into lyotropic liquid crystalline

phases. These amphiphiles play the role of classical surfactants such as for emulsification but because of their nanoparticle headgroups, also act as catalysts for chemical reactions.

Cheng and collaborators [45–48] have introduced the terminology of "molecular nanoparticles" to suggest that the nanoparticles can be viewed as molecules and the terminology of "giant surfactants" to represent the amphiphiles composed of compact and rigid nanoparticles as the headgroup and flexible polymer chains as tail (Figure 1.9a,b). Examples of such giant amphiphiles studies in their laboratory include those based on functionalized fullerene, polyhedral oligomeric silsesquioxanes (POSS), and POM derivatives, with variable surface functionalities. They have also constructed amphiphiles where both the head and tail groups are nanoparticles by combining fullerene as the hydrophobic tail with functionalized fullerene as the hydrophilic head (Figure 1.9c,d).

Yu et al. [45] found that AC_{60}-PS_n (polystyrene with block size n) amphiphiles (Figure 1.9a) formed spherical micelles at low concentrations while at higher concentrations they transformed into cylindrical micelles and vesicles depending on the chain length of the hydrophobic polystyrene block. The concentration effect was attributed to the increasing concentration of protons in solution leading to reduction in the carboxylic acid dissociation and the net charge on the headgroup. The AC_{60}-$2PS_n$ amphiphiles (Figure 1.9b) aggregated into vesicles. These results can be readily explained qualitatively by the free energy model given by Eq. (1.21).

Lin et al. [48] found that the AC_{60}-C_{60} and AC_{60}-$2C_{60}$ amphiphiles (Figures 1.9c,d) made up of nanoparticles as both the hydrophobic head and the hydrophilic tail also self-assembled into various morphologies when studied in either tetrahydrofuran (THF) or dimethyl formamide (DMF)-water mixture as solvents. They found that in THF, vesicles were formed for AC_{60}–C_{60} and AC_{60}–$2C_{60}$, but with different inter layer packing arrangements. In the DMF/water system, spherical, and cylindrical micelles were formed for AC_{60}–C_{60} and AC_{60}–$2C_{60}$, respectively. The authors have suggested that in THF as the solvent, the dissociation of carboxylic acid is small and therefore the electrostatic headgroup repulsions are small. As a result, the area per molecule will be small, the packing parameter will be large, and vesicles are expected. In contrast, in DMF/water, the dissociation of the carboxylic acid will be larger and therefore the headgroup repulsions will be of larger magnitude. As a consequence, the area per molecule will be larger, the packing parameter will be smaller, and cylindrical and spherical micelles are thus formed. These interpretations are consistent with the application of the free energy models developed for the classical amphiphilic systems, with accounting made for the geometrical properties of the nanoparticle head and tail groups.

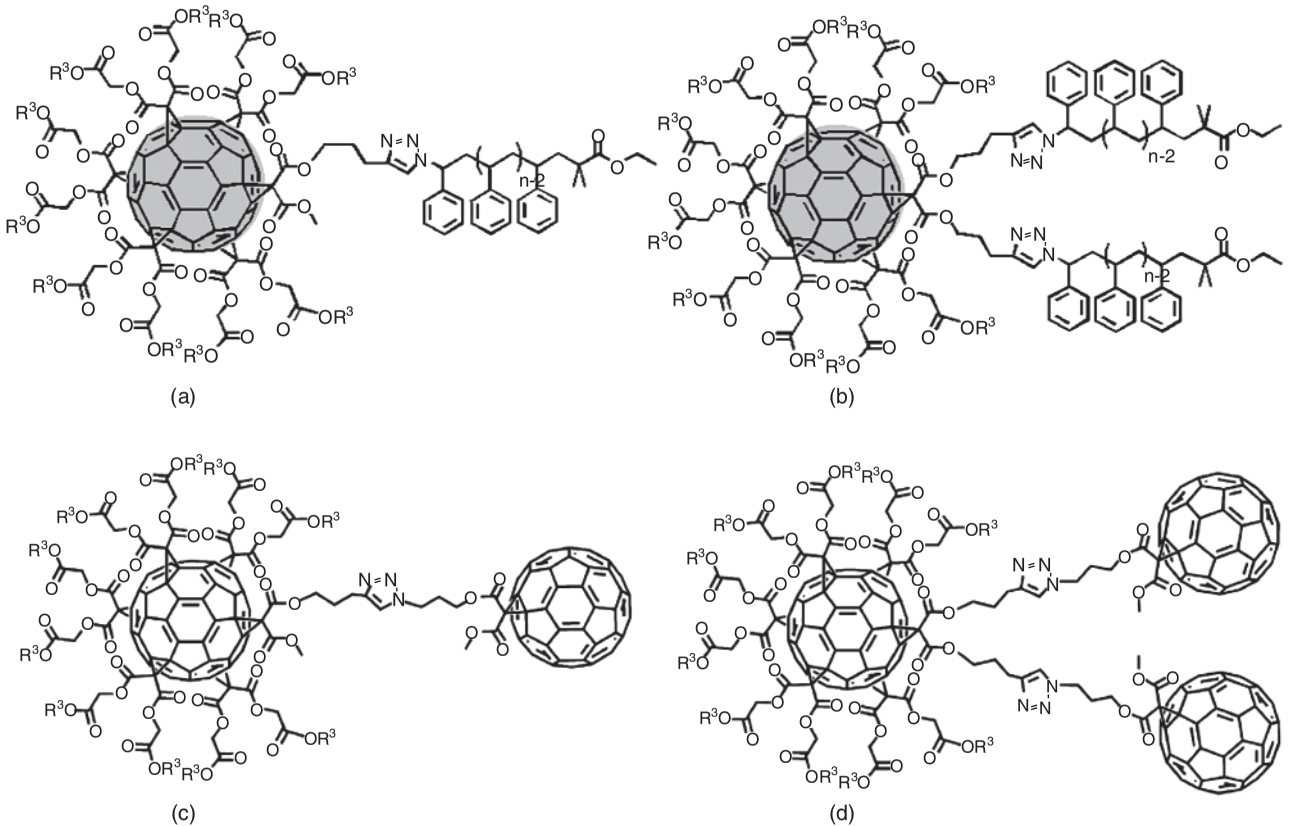

Figure 1.9 Structures of some of the nanoparticle amphiphiles synthesized and studied in Cheng laboratory. Shown are amphiphiles with hydrophilic AC_{60} headgroup and with one (a) or two (b) hydrophobic polystyrene tails. A new class of giant molecules have also been created with hydrophilic AC_{60} and hydrophobic C_{60}. Shown are such giant molecules with one (c) hydrophobic C_{60} or two (d) hydrophobic C_{60}. The notation AC_{60} represents C_{60} Fullerene functionalized with 10 carboxylic acid groups and A denotes the carboxylic acid functionality. Cheng et al. discuss in detail such nanoparticle amphiphiles they have created in Chapter 10 of this book.

1.4 Conclusions

Studies of self-assembly in solutions over almost a century have focused on surfactants and block copolymer molecules forming aggregates of various shapes. Although surfactants and block copolymers exhibit analogous self-assembly behavior, the two fields have evolved independent of one another, with the theoretical models emphasizing mutually exclusive molecular features. In the Tanford model for surfactant micelle, the balancing of surfactant headgroup repulsions against the interfacial energy determines the equilibrium properties of the aggregate. Noticeably absent was any influence attributed to the hydrophobic tail over the aggregate size and shape. In the de Gennes model for block copolymer micelle, the micelle characteristics are determined by the balancing of elastic deformation of the solvophobic block against the interfacial energy. The solvophilic block interactions (which are the analog of the surfactant headgroup interactions) play no role in determining the micelle characteristics. By incorporating the mutually neglected free energy contributions between these two theoretical models, we can have a unitary theory applicable to both surfactants and block copolymers. The incorporation of surfactant tail deformation free energy by borrowing from the block copolymer model has led to more accurate predictions of the critical micelle concentration and micelle characteristics for many classical surfactants. Similarly, the incorporation of solvophilic block interactions by borrowing from the surfactant model provides predictions about block copolymer micelles that are consistent with experiments that demonstrate the significant influence of the solvophilic block.

The free energy models of surfactants and block copolymers can be adapted and extended to account for interactional terms connected to novel headgroups such as peptides, oligonucleotides, POSS, POM, etc., and also to account for novel hydrophobic tails such as hydrophobic peptides, fullerenes, etc., in order to quantitatively describe the wide pattern of aggregation observed in these nonclassical amphiphilic systems. The design of such novel amphiphiles incorporating responsiveness and programmability and the ability to combine organic, inorganic, and biological moieties within a single molecular structure makes this area a very interesting and fertile field of research for years to come. The novel amphiphiles make possible entirely new areas of applications in materials science and nanomedicine, far beyond the traditional colloidal applications of surfactants and block copolymers.

Acknowledgments

Support from Natick Soldier Research, Development and Engineering Center, is acknowledged.

References

1 McBain, J.W. (1913). General discussion on colloids and their viscosity. *Trans. Faraday Soc.* 9: 99–101.
2 Hartley, G.S. (1936). *Aqueous Solutions of Paraffin Chain Salts*. Paris: Hermann et Cie.
3 Debye, P. (1949). Light scattering in soap solutions. *J. Phys. Colloid Chem.* 53: 1–8.
4 Nagarajan, R. (2014). One hundred years of micelles: evolution of the theory of micellization. Chapter 1. In: *Surfactant Science and Technology: Retrospects and Prospects* (ed. L.S. Romsted), 3–52. Boca Raton, FL: Taylor and Francis.
5 Dunn, A.S. and Melville, H.W. (1952). Synthesis of 'block' copolymers. *Nature* 169: 699–700.
6 Merrett, F.M. (1957). Graft polymers with preset molecular configurations. *J. Polym. Sci.* 24: 467–477.
7 Climie, I.E. and White, E.F.T. (1960). The aggregation of random and block copolymers containing acrylonitrile in mixed solvents. *J. Polym. Sci.* 47: 149–156.
8 Krause, S. (1964). Dilute solution properties of a styrene-methyl methacrylate block copolymer. *J. Phys. Chem.* 68: 1948–1955.
9 Riess, G. (2003). Micellization of block copolymers. *Prog. Polym. Sci.* 28: 1107–1170.
10 Tanford, C. (1973). *The Hydrophobic Effect*. New York: Wiley.
11 Israelachvili, J.N., Mitchell, J.D., and Ninham, B.W. (1976). Theory of self-assembly of hydrocarbon amphiphiles into micelles and bilayers. *J. Chem. Soc., Faraday Trans. 2* 72: 1525–1568.
12 Meier, D.J. (1969). Theory of block copolymers. I. Domain formation in A-B block copolymers. *J. Polym. Sci. C* 26: 81–98.
13 Meier, D.J. (1970). A theory of the morphology of block copolymers. *Polym. Prepr.* 11: 400–405.
14 Helfand, E. and Tagami, Y. (1971). Theory of the interface between immiscible polymers. *J. Polym. Sci., Part B: Polym. Lett.* 9: 741–746.
15 Helfand, E. and Sapse, A.M. (1975). Theory of unsymmetric polymer-polymer interfaces. *J. Chem. Phys.* 62: 1327–1331.
16 de Gennes, P.G. (1978. . Suppl. 14). Macromolecules and liquid crystals: reflections on certain lines of research. In: *Solid State Physics* (ed. J. Liebert), 1–18. Academic Press.
17 Leibler, L., Orland, H., and Wheeler, J.C. (1983). Theory of critical micelle concentration for solutions of block copolymers. *J. Chem. Phys.* 79: 3550–3557.
18 Noolandi, J. and Hong, K.M. (1983). Theory of block copolymer micelles in solution. *Macromolecules* 16: 1443–1448.

19 Whitmore, M.D. and Noolandi, J. (1985). Theory of micelle formation in block copolymer- homopolymer blends. *Macromolecules* 18: 657–665.

20 Tanford, C. (1974). Theory of micelle formation in aqueous solutions. *J. Phys. Chem.* 78: 2469–2479.

21 Nagarajan, R. and Ruckenstein, E. (1991). Theory of surfactant self-assembly: a predictive molecular thermodynamic approach. *Langmuir* 7: 2934–2969.

22 Nagarajan, R. (2002). Molecular packing parameter and surfactant self-assembly: the neglected role of the surfactant tail. *Langmuir* 18: 31–38.

23 Semenov, A.N. (1985). Contribution to the theory of microphase layering in block-copolymer melts. *Sov. Phys. JETP* 61: 733–742.

24 Daoud, M. and Cotton, J.P. (1982). Star shaped polymers – a model for the conformation and its concentration-dependence. *J. Phys.* 43: 531–538.

25 Zhulina, Y.B. and Birshtein, T.M. (1985). Conformations of molecules of block copolymers in selective solvents (Micellar structures). *Polym. Sci. USSR* 27: 570–576. (Original article in Russian published in Vysokomol. Soyed. A27: No. 3, 511–517, 1985).

26 Halperin, A. (1987). Polymeric micelles – a star model. *Macromolecules* 20: 2943–2946.

27 Nagarajan, R. and Ganesh, K. (1993). Solubilization in spherical block copolymer micelles: scaling analysis based on star model. *J. Chem. Phys.* 98: 7440–7450.

28 Flory, P.J. (1962). *Principles of Polymer Chemistry*. Ithaca, NY: Cornell University Press.

29 Nagarajan, R. and Ganesh, K. (1989). Block copolymer self-assembly in selective solvents – spherical micelles with segregated cores. *J. Chem. Phys.* 90: 5843–5856.

30 Nagarajan, R. and Ganesh, K. (1989). Block copolymer self-assembly in selective solvents – theory of solubilization in spherical micelles. *Macromolecules* 22: 4312–4325.

31 Nagarajan, R. and Ganesh, K. (1996). Comparison of solubilization of hydrocarbons in (PEO–PPO) diblock versus (PEO–PPO–PEO) triblock copolymer micelles. *J. Colloid Interface Sci.* 184: 489–499.

32 Nagarajan, R. (1996). Solubilization of hydrophobic substances by block copolymer micelles in aqueous solutions. In: *Solvents and Self-Organization of Polymers*, NATO ASI Series, vol. 327 (ed. S.E. Webber, P. Munk and Z. Tuzar), 121–165. Kluwer Publishers.

33 Lettow, J.S., Lancaster, T.M., Glinka, C.J. et al. (2005). Small-angle neutron scattering and theoretical investigation of poly(ethylene oxide)-poly(propylene oxide)-poly(ethylene oxide) stabilized oil-in-water microemulsions. *Langmuir* 21: 5738–5746.

34 Thota, B.N.S., Berlepsch, H.v., Böttcher, C. et al. (2015). Towards engineering of self-assembled nanostructures using non-ionic dendritic amphiphiles. *Chem. Commun.* 51: 8648–8651.

35 Thompson, M.P., Chien, M.-P., Ku, T.-H. et al. (2010). Smart lipids for programmable nanomaterials. *Nano Lett.* 10: 2690–2693.

36 Peterson, A.M. and Heemstra, J.M. (2015). Controlling self-assembly of DNA-polymer conjugates for applications in imaging and drug delivery. *WIREs Nanomed. Nanobiotechnol.* 7: 282–297.

37 Kedracki, D., Safir, I., Gour, N. et al. (2013). DNA–polymer conjugates: from synthesis, through complex formation and self-assembly to applications. *Adv. Polym. Sci.* 253: 115–150.

38 Shimada, T., Sakamoto, N., Motokawa, R. et al. (2012). Self-assembly process of peptide amphiphile worm-like micelles. *J. Phys. Chem. B* 116: 240–243.

39 Xu, H., Wang, J., Han, S. et al. (2009). Hydrophobic-region-induced transitions in self-assembled peptide nanostructures. *Langmuir* 25: 4115–4123.

40 Ku, T.-H., Chien, M.-P., Thompson, M.P. et al. (2011). Controlling and switching the morphology of micellar nanoparticles with enzymes. *J. Am. Chem. Soc.* 133: 8392–8395.

41 Boyer, C., Huang, X., Whittaker, M.R. et al. (2011). An overview of protein–polymer particles. *Soft Matter* 7: 1599–1614.

42 Landsmann, S., Lizandara-Pueyo, C., and Polarz, S. (2010). A new class of surfactants with multinuclear, inorganic headgroups. *J. Am. Chem. Soc.* 132: 5315–5321.

43 Li, W. and Gunton, J.D. (2013). Self-assembly of Janus ellipsoids II: Janus prolate spheroids. *Langmuir* 29: 8517–8523.

44 Wen, J., Yuan, L., Yang, Y. et al. (2013). Self-assembly of monotethered single-chain nanoparticle shape amphiphiles. *ACS Macro Lett.* 2: 100–106.

45 Yu, X., Zhang, W.-B., Yue, K. et al. (2012). Giant molecular shape amphiphiles based on polystyrene–hydrophilic [60] fullerene conjugates: click synthesis, solution self-assembly, and phase behavior. *J. Am. Chem. Soc.* 134: 7780–7787.

46 Yu, X., Li, Y., Dong, X.-H. et al. (2014). Giant surfactants based on molecular nanoparticles: precise synthesis and solution self-assembly. *J. Polym. Sci., Part B: Polym. Phys.* 52: 1309–1325.

47 Zhang, W.-B., Yu, X., Wang, C.-L. et al. (2014). Molecular nanoparticles are unique elements for macromolecular science: from "nanoatoms" to giant molecules. *Macromolecules* 47: 1221–1239.

48 Lin, Z., Lu, P., Hsu, C.-H. et al. (2014). Self-assembly of fullerene-based Janus particles in solution: effects of molecular architecture and solvent. *Chem. Eur. J.* 20: 11630–11635.